LAPPEENRANTA UNIVERSITY OF TECHNOLOGY

LUT School of Energy Systems

Master's Degree Program in Electrical Engineering

SOLAR POWER PRODUCTION FORECAST BASED ON WEATHER DATA IN FINLAND

Examiners: Professor Jero Ahola

Associate Professor Antti Kosonen

Author: Mrecha Amani Metta

Abstract

Lappeenranta University of Technology
School of Energy Systems
Degree Program in Electrical Engineering

Mrecha Amani Metta

Solar Power Production Forecast Based on Weather Data in Finland

2017

Master's Thesis
67 pages, 38 Figures, 6 Tables, 3 Appendices

Examiners: Professor Jero Ahola
Associate Professor Antti Kosonen

Keywords: solar power forecasting, solar irradiation, Numerical Weather Prediction (NWP), Photovoltaic (PV) system, Normalized Root Mean Square Error (NRMSE).

Solar power forecasting has become an important factor in Europe in the recent past, particularly in the middle Europe as well as in the Nordic countries such as Denmark and Finland. The need for accurate forecasting has played a pivotal role in planning the operations of photovoltaic (PV) systems as well as in achieving power grid balance. In this thesis, a statistical model for solar power forecasting is computed, studied, investigated and used to predict solar power. The model uses past power measurements and meteorological forecasts of temperature, solar irradiation, relative humidity and wind speed as inputs. The weather forecast parameters used to compute power are obtained from Aladin Research Model on Non-hydrostatic forecast Inside Europe (HARMONIE) representing Lappeenranta region. The computed estimate power is then compared with the real power produced from Lappeenranta University of Technology (LUT) solar power plant. Normalized Root Mean Square Error (NRMSE) is used as the evaluation criteria.
The results indicate that solar power production can be forecasted using the model with small NRMSE errors captured indicating better performance of the model.

Acknowledgements

This thesis was given by Lappeenranta University of Technology (LUT). Firstly, I would to like to thank my supervisor, Professor Jero Ahola and Antti Kosonen for their great support and guidance throughout my thesis. Their availability and provision of much needed supervision has been of immense help.

Secondly, I would like to thank Professor Anders Lindfors from Finnish Meteorological Institute (FMI) for his contribution in my thesis, especially in providing the meteorological data used in my thesis.

Thirdly, I would like to thank my friends, especially Arun Bhattarai and Fred Ndyamukama, for all your support not only in my thesis but also in other life endeavors.

Finally, I would like to thank my family for their unrelenting support, love and the source of inspiration they have been to me. I'm grateful for having you.

Lappeenranta 20.06.2017

Mrecha Amani Metta.

Table of contents

Appendices

Abbreviations

ARIMA	Time series Auto Regressive Integrated Moving Average
AC	Alternating Current
AEMET	Agencia Estatal de Meteorology
CIGS	Copper Indium Gallium Diselemide
CdTe	Cadmium Telluride
CT	Civil Time
DMI	Danish Meteorological Institute
DC	Direct Current
DHI	Direct Horizontal Irradiation
EMHI	Estonian Meteorological and Hydrological Institute
EEA	European Environmental Agency
ECMWF	European Centre for Medium-Range Weather Forecast
EU	European Union
EPIA	European Photovoltaic Industry Association
FMI	Finnish Meteorological Institute
FF	Fill Factor
GHG	Green House Gas
GMT	Greenwich Mean Time
GHI	Global Horizontal Irradiation
HARMONIE	Aladin Research Model On Non-hydrostatic forecast Inside Europe
HIRLAM	High Resolution Limited Area Model
HDKR	Hay Davis Klucher Reindl
IEA	International Energy Agency
IMI	Icelandic Meteorological Institute
KNMI	Royal Netherlands Meteorological Institute
LMHS	Lithuania Norwegian Meteorological Institute
LUT	Lappeenranta University of Technology
MPP	Maximum Power Point
MET	Norwegian Meteorogical Institute

MST	Mean Solar Time
MAE	Mean Absolute Error
NWP	Numerical Weather Prediction
NOCT	Normal Operating Cell Temperature
NRMSE	Normalized Root Mean Square Error
PV	Photovoltaic
PCT	Pew Chartable Trust
RST	Real Solar Time
RMSE	Root Mean Square Error
STC	Standard Test Condition
SMHI	Swedish Meteorological and Hydrological Institute
TD	Time Difference
UT	Universal Time
UTC	Coordinated Universal Time

Symbols

A_i	anisotropy index
A	area of PV panel
f	modulating factor
I_b	direct horizontal irradiation
I_d	diffuse horizontal irradiation
I_0	extraterrestrial horizontal irradiation
I_T	total irradiation on tilted surface
I_{ph}	photo-current
I_{sc}	short circuit current
I_g	global horizontal irradiation
$long$	longitude
n	number of the day
N	total number observation in time horizon
P_{PV}	estimated power output

$P_{LUT.Realpower}$	real power
$P_{HARM.Forecast}$	forecast power
$P_{install}$	power capacity installed
R_{sh}	shunt resistance
R_s	series resistance
R_b	tilt factor for beam irradiation
T_a	air temperature
T_c	panel temperature
T_{STC}	panel temperature at standard test condition
U_{PV}	heat exchange coefficient
v_w	local wind speed
v_f	wind speed close to solar panel
V_{oc}	open circuit voltage
W_p	watt peak

Greek Symbols

γ	surface azimuth angle
β	panel tilt angle
δ	declination angle
ϕ	latitude angle
η_{PV}	solar panel efficiency
θ_z	zenith angle
γ_s	solar azimuth angle
ρ_g	ground reflected
β_{STC}	temperature coefficient at maximal power
$\tau.\alpha$	transmittance absorptance product
α_s	altitude angle
ω	hour angle
θ	angle of incidence

1. Introduction

This section provides the research problem statement and a brief description about the research objective. In addition, the motivation of conducting this research is presented in this section. Finally, the structure of this thesis is outlined.

1.1. Research problem

The need to diversify the energy production has increased recently. This can be attributed to the up-surging demand in the consumption of energy ranging from large consumers inter alia commercial industries to small energy consumers such as normal households. As a result, a combined effort from different stakeholders ranging from individuals, researchers, to institutions and other interested parties have embarked on how to integrate energy sources into energy grid. Real power production for instance has been a common source of energy notwithstanding its cost of production and some environmental challenges it may pose. Renewable energy has emerged as another source of energy owing to its environmental-friendliness. Even more, combination of both these sources have been found to complement each other. The ability to forecast energy production and its consumption has been found to be of paramount importance. As such, this thesis aims to examine further the production and forecasting of power energy production from the weather parameters.

1.2. Objective of the thesis

The goal of this thesis is to forecast power energy based on weather conditions provided by Numerical Weather Prediction (NWP) model. The weather parameters used in this thesis as obtained from HARMONIE model weather station for Lappeenranta region include temperature, wind speed, humidity and solar irradiation. The need to forecast power production is a critical phenomenon regarding the efficient and effective production and consumption of the same.

The objective of the thesis is further divided into two categories namely:

- Computation of estimated power output forecast which is derived from the weather parameters comprising temperature and wind speed and total solar irradiation from HARMONIE model. The calculation of total solar irradiation is accomplished by considering the beam horizontal irradiation, diffuse horizontal irradiation and global horizontal irradiation.

- Comparing the obtained power output forecast with the real power produced from the power production plant from Lappeenranta University of Technology (LUT).

1.3. Research motivation

The constant increase in world population and the corresponding increase in electricity consumption is foreseen to double by the year 2050 (IEA, 2009). It is estimated that primary energy demand worldwide will increase by 45% and the demand for electricity will also go up to 80% between 2006 and 2030 (IEA, 2009). As a result, in the absence of severe precautions, the rate of Green House Gas (GHG) is expected to double by 2050 (IEA, 2009). In addition, the demand for oil will also rise and thereby affecting its supply security. There are separate ways towards balancing GHG concentrations, but the main alternative under consideration is the replacement of fossil fuels with various forms of renewable energy sources (IEA, 2009).

The European dependence on imported fossil fuel (crude oil, natural gas and coal) from non-EU countries as primary share of energy consumption went up from 50.8% in 2000 to 54.2% in 2005 (EEA, 2008). Furthermore, the baseline scenarios indicate that there is an increasing dependency in fossil fuel requirement from 50% in 2005 up to 84% by 2030. To reverse these conditions, the European countries made the decision to reduce their requirement of nuclear energy and agreed to limit the target consumption of electricity to 20% as a supply from renewable energy sources by 2020 (EEA, 2008). Under this commitment, it is envisaged that at least 20% reduction of GHG emission by 2020 can be achieved, compared to 1990 levels (Union, 2009).

Solar and wind power are currently seen as the main renewable energy sources prioritized to compete with production of fossil fuel energy in the future (WIRE, 2010). Therefore, the current focus on solar and wind energy potential is to forecast the intermittent renewable energy forms according to weather conditions. Together with the development of electric grid management, solar and wind energy forecasting is pivotal in aiding in the installations of renewable energy plants. These forecasts will also help grid operators to manage the energy production more efficiently. The goal of EU deal is to allow increased transmission of renewable energy between the cooperating countries. As research has indicated, critically studying the solar irradiation in EU can help enhance the availability of solar energy as an

alternative source of renewable energy (WIRE, 2010). As such, this forms the basis from which this thesis is inspired.

1.4. Structure of the thesis

In addition to the aforementioned sections, this thesis is subsequently divided into six sections. Section (2) provides the related literature that forms the basis of this research. Section (3) presents the research methodology from which the results of this study are obtained. Thereafter, Section (4) outlines the findings of this thesis. A subsequent description of the results is provided in Section (5). Finally, Section (6) provides the concluding remarks.

2. Literature review

This section provides the related literature pertaining this thesis particularly but not limited to solar irradiation and solar power forecasting.

2.1. Review of solar irradiation and power forecasting

Solar irradiation is one of the most important input parameter of Photovoltaic (PV) Power output. Forecasting of solar irradiation precisely using Numerical Weather Prediction (NWP) can guide in the estimation of power output.

According to Lorenz et al. (2009), the approach of solar irradiance forecasting is one of the main basis of Photovoltaic (PV) power prediction. Duffie and Beckman (2013) defines solar irradiation as the incident energy per unit area on surface which can be obtained by integration of irradiation over a specified time ranging from an hour to a day.

Solar irradiation forecasting has been utilized in various scenarios. Most notably, together with Numerical Weather Prediction, solar irradiation forecasting has been used to accurately compare estimated power output and the real power production. For instance, according to Pelland et al. (2013), solar irradiation has been used in the Global Environmental Multiscale Model in Canada to forecast the hourly solar and photovoltaic forecasts with remarkable success. The model has used the global numerical weather predictions model as opposed to observation methods with the former believed to suit best longer forecasts horizon (Pelland et al., 2013).

In Germany, as the efforts towards integration of renewable energy into energy supply system is gaining traction, attention is being paid on the need to forecast the availability of the renewable energy, especially the solar and wind energy (Lorenz et al., 2011). This integration of fluctuating renewable energies is believed to alter the load profiles thus the need of their forecast so as to adjust the respective load forecasts. Commencing with forecasting of the global horizontal irradiance, which is considered the most crucial step in PV power prediction systems, Germany has developed power prediction system particularly for the universities of Oldenburg and Meteocontrol with a forecast horizon of 2-days ahead with hourly resolution (Lorenz et al., 2011).

Similarly, as presented by Lorenz et al. (2009), different approaches to forecast solar irradiance with the use of NWP models have been developed and compared in various parts of Europe, with Germany, Austria, Switzerland and Spain being among the countries involved.

Of importance from these approaches is the forecast of the horizontal global irradiance which is then converted according to the orientation and declination of the panels to model the irradiance (Lorenz et al., 2009).

Yang et al. (2012) has portrayed the possibility of forecasting an hour ahead solar irradiation. In their research, three-pronged approach has been utilized in forecasting solar irradiance based on meteorological data including global horizontal irradiance, diffuse horizontal irradiance, direct normal irradiance, and cloud cover. Time series Auto Regressive Integrated Moving Average (ARIMA) has been used to forecast solar irradiation in this research (Yang et al., 2012).

Similar studies pertaining the forecast of power output have been conducted in the United States of America. In American Southwest to be precise, Research conducted by Larson et al. (2016), has emphasized on the forecasting of power output from photovoltaic power plants. As indicated from the results, bias errors in the irradiance input have limited impact on the power output performance. This is quantified by the Root Mean Square Error (RMSE) captured as ranging from 10.3% to 14% of the capacity (Larson et al., 2016).

As Yona et al. (2007) notes, the introduction of alternative energy source for example the solar energy is inevitable in the recent years. In addition, it is noted that, the output of photovoltaic system is influenced by meteorological conditions. In their research, Artificial Neural Network is used to predict the insolation of the solar system, whose estimation is believed to accurately predict the power output of photovoltaic system (Yona et al., 2007).

Similar researches have continued to show the importance of integration of other renewable energy sources into the energy grid with the ability of forecasting playing a critical role. As corroborated by Bacher et al. (2009) various models can ease the solar power forecasting. A casing point as indicated in their study, is the online forecasting approach of production from photovoltaic systems (Bacher et al., 2009). Based on this approach values of solar power are predicted for horizons of up to 36 hours. To aid in this process, Auto Regressive (AR) and Auto Regressive with Exogenous input (ARX) are used. The ARX model takes the Numerical Weather Predictions (NWPs) as its input. According to their results, NWPs are necessary inputs for longer forecasts horizon (Bacher et al., 2009).

As indicated in this literature, various forecast models pertaining the forecast of solar energy mostly depend on weather data. Because of the fluctuating tendency of the weather parameters, it is of paramount importance to forecast the energy output, thus providing efficient and effective structuring, management and planning of the energy grid. The provision of accurate data from these forecasts aid in improving performance of integrated energy grid.

In addition, current studies are based on forecast, and limited studies have focused on discovering the potential of forecast methods at the level of the system. System level forecasts can be useful to system operators to make better informed arrangements pertaining energy production, distribution and consumption. In addition, with the expansion of PV system within the electricity market, this forecast can help all participant to improve their bid strategy.

2.2. Potential of solar energy in Finland

Owing to its benefits, solar energy is envisaged to be a major contributor as a source of renewable energy in the future (Haukkala, 2015). The fact that it is environmental friendly with innocuous emissions, together with its low management and maintenance cost makes solar energy a better choice as a source of renewable energy. Most importantly, due to its omnipresence globally, its availability cannot therefore be restrained by ownership constraints as opposed to other sources of energy such as fossil fuel (Haukkala, 2015). Indeed, according to the International Energy Agency (IEA), solar energy could be the largest source of electricity by 2050 (IEA, 2014).

As such, solar energy has attracted considerable attention globally. Various countries around the world has continued garnering efforts towards harnessing this energy source. This includes but not limited to structuring, managing and maintaining the energy source, integrating it with the energy system grid as well as providing solar energy support polices and the devising and implementation of the usage strategies.

Countries ranging from Asia with China as a case in point to Europe with Germany and/or the United Kingdom (UK) as examples have continued to use solar energy (EPIA, 2014). Notwithstanding the benefits of solar energy, not every other country has emphasized on its use. For instance, the use of solar energy in Nordic Countries has been relatively limited compared to other source of renewable energies (Haukkala, 2015). Particularly, not only has been the use of solar energy been low in Finland but also the position of solar technology

has been weak. This is contrary to the fact that the focus on Photovoltaics (PV) has been drastically increasing over period of time across the globe.

Despite solar energy outweighing other clean energy technologies in terms of generating capacity, according to Pew Charitable Trusts (PCT), Finland has reluctantly implemented any subsidy in the use of solar energy (Initiatives, 2014). Nevertheless, energy consumption per capita in the country has been one of the highest among the industrial countries owing to the substantial number of energy-intensive industries, the cold climate and the sparsely fragmented populated structures (Värttö & Ahoniemi, 2009). In addition, various researches have indicated the Country's potential to utilize solar energy. For example, according to Breyer et al. (2017), the variation of solar irradiation potential between Finland and Germany, which is considered the European top market in terms of solar energy, doesn't differ significantly as illustrated in both Figure 1 and 2. This therefore begs the question, why the failure to adopt the solar energy support policy in Finland?

In their work, Haukkala et al, (2015) has attributed this failure to several barriers ranging from technological, economical, and institutional. Furthermore, the technological barriers can be attributed to the economical, political and behavioral aspects (Sovacool, 2009). In other words, in addition to the general attitude of people objecting to change, the proponents of wind and solar of energy perceive the solar energy technologies as radical ones thus the decline in motivation.

However, the work of Child and Breyer (Child & Breyer, 2016) has revisited and expanded the results of Haukkala (Haukkala, 2015). According to the former, indeed the solar PV in Finland can be an integral part of a competitive future energy systems, consequently creating a space for challenging other barriers to maximum utilization of solar energy with the exception of the technical and the regulatory ones.

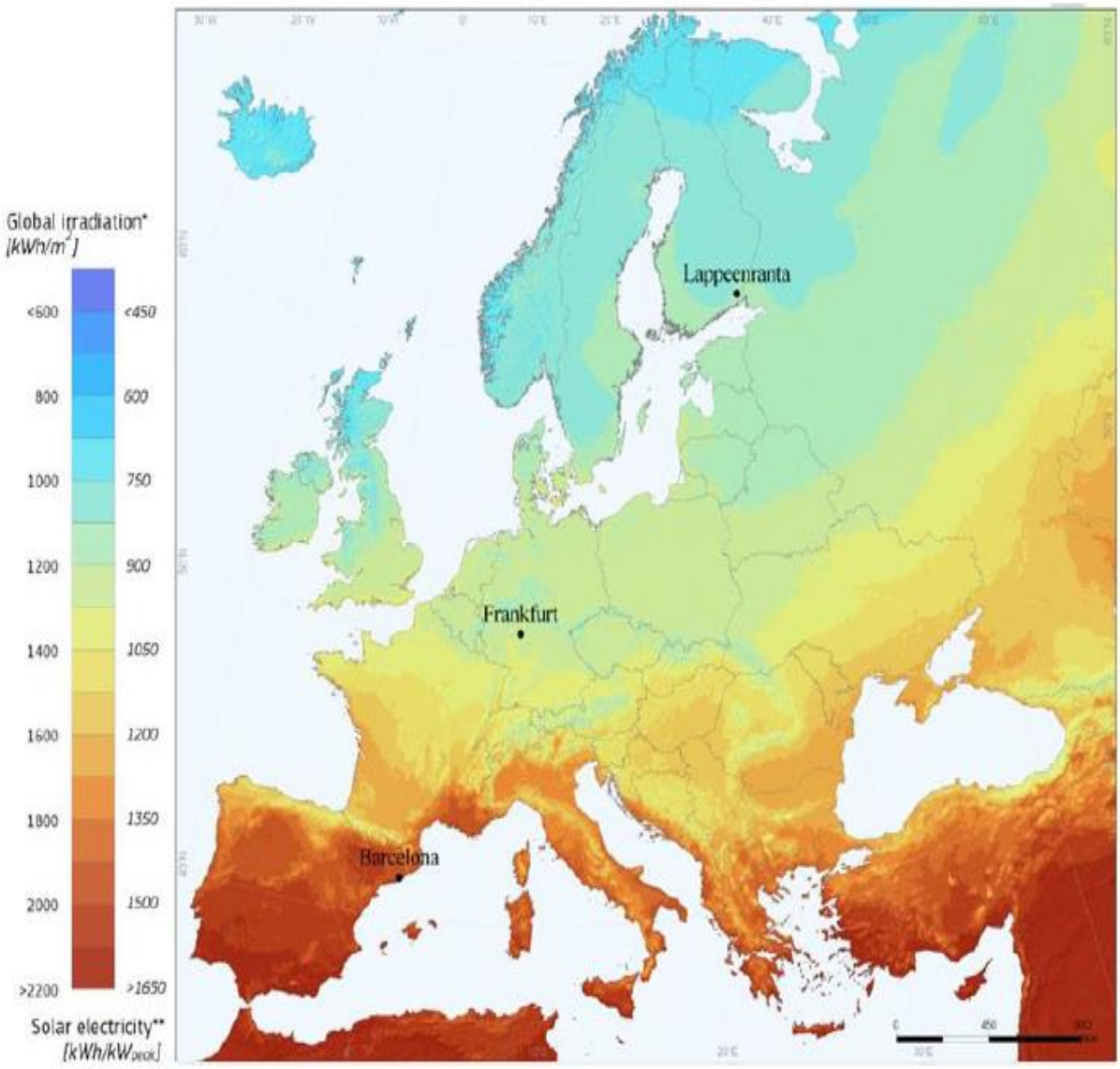

Figure 1: Solar power production potential in Europe. *Yearly sum global irradiation potential in European countries (Huld & Pascua, 2014).

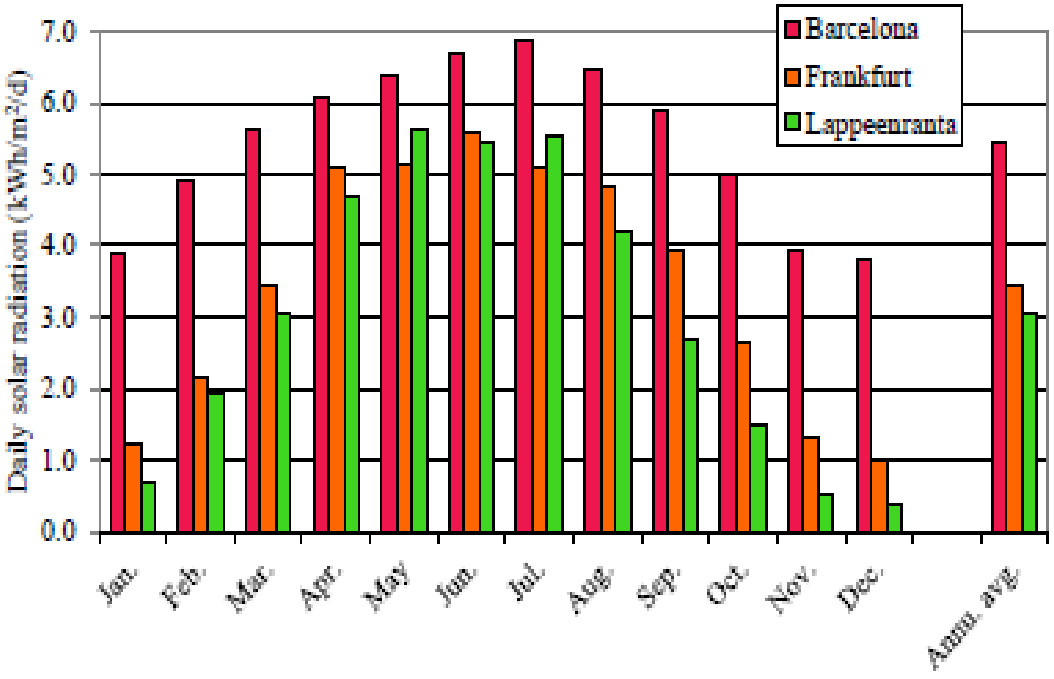

Figure 2: Solar irradiation potential in European countries (Kosonen et al, 2014).

3. Research methodology

In this section, the steps in modelling the computation of the forecasted solar power are demonstrated, in addition to the due process of comparison with the real power produced from the LUT power plant.

This section involves working with numerical data available from separate data sets. As depicted in Figure 3, various input parameters have been considered in computation of the power output. Most importantly, the weather conditions comprising of solar irradiation, air temperature and wind speed have been used among the input parameters. The weather conditions have been obtained from HARMONIE model. The HARMONIE model is a Numerical Weather Prediction (NWP) model that came as result of cooperation between the High Resolution Limited Area Model (HIRLAM), a forecast system developed by international HIRLAM programme (http://en.ilmatieteenlaitos.fi/). Subsequently, HIRLAM programme is a cooperation various European meteorological institutes including Danish Meteorological Institute (DMI) Denmark, Estonian Meteorological and Hydrological Institute (EMHI) Estonia, Finnish Meteorological Institute (FMI) Finland, Icelandic Meteorological Institute (IMI), Iceland, Lithuanian Hydrological and Meteorological Services (LHMS) Lithuania, Norwegian Meteorological Institute (MET), Norway, Royal Netherlands Meteorological Institute (KNMI) (The Netherlands), Agencia Estatal de Meteorology (AEMET) and Swedish Meteorological and Hydrological Institute (SMHI) (Sweden).

The choosing of the weather data was influenced by the power production data from the LUT power plant (https://www.lut.fi/web/en/green-campus/green-campus-in-numbers/production-figures). The weather data chosen represented time series hourly data from the 21/05/2016 to 27/05/2016. The rationale for choosing the data on the prescribed date was influenced by the fact that power production from LUT power plant was stable during those days. In addition, in those days the weather data was observed not to be fluctuating a lot. The weather data was also selected from 27/08/2016 to 02/09/2016 so as to also have representation of the model during the rainy seasons. The weather data needed to be in close proximity to the LUT power plant and as such Lappeenranta University of Technology (LUT) weather station was selected at latitude 61°.066´N and longitude 28°.091´E respectively. It is worth noting that the weather data were the parameter inputs used to calculate the estimate power output.

Power production data was obtained from Lappeenranta University of Technology (LUT) power production plant for both the time series ranging from 21/05/2016 to 27/05/2016 and from 27/08/2016 to 02/09/2016.The selected hourly data was to be in tandem with the weather data. As it was observed, solar energy production is affected during cloudy and rainy days where solar irradiation is believed to be limited. The efficient and surface area of the panel are considered from the panel to give the output.

The computation of the incident of the solar irradiation on the panels ensued which was based on the sun position and the panels orientation. In addition, the total solar irradiation was achieved by considering sunlight components including global, beam and diffuse irradiation.

Another vital component was the solar panel operating temperature which was based on the air temperature, total solar irradiation, wind speed, heat fluxes from the ground surface and system materials. Consequently, the computation of the power output from the forecast model considered the solar irradiation and panel operating temperature. Owing to the fact that, the forecasted power output was derived in Direct Current (DC), there was a need to convert it to Alternating Current (AC) thus coinciding with the solar power AC from the solar production plant for easier comparison. As a result, the forecast power output and the efficiency of the inverter were considered.

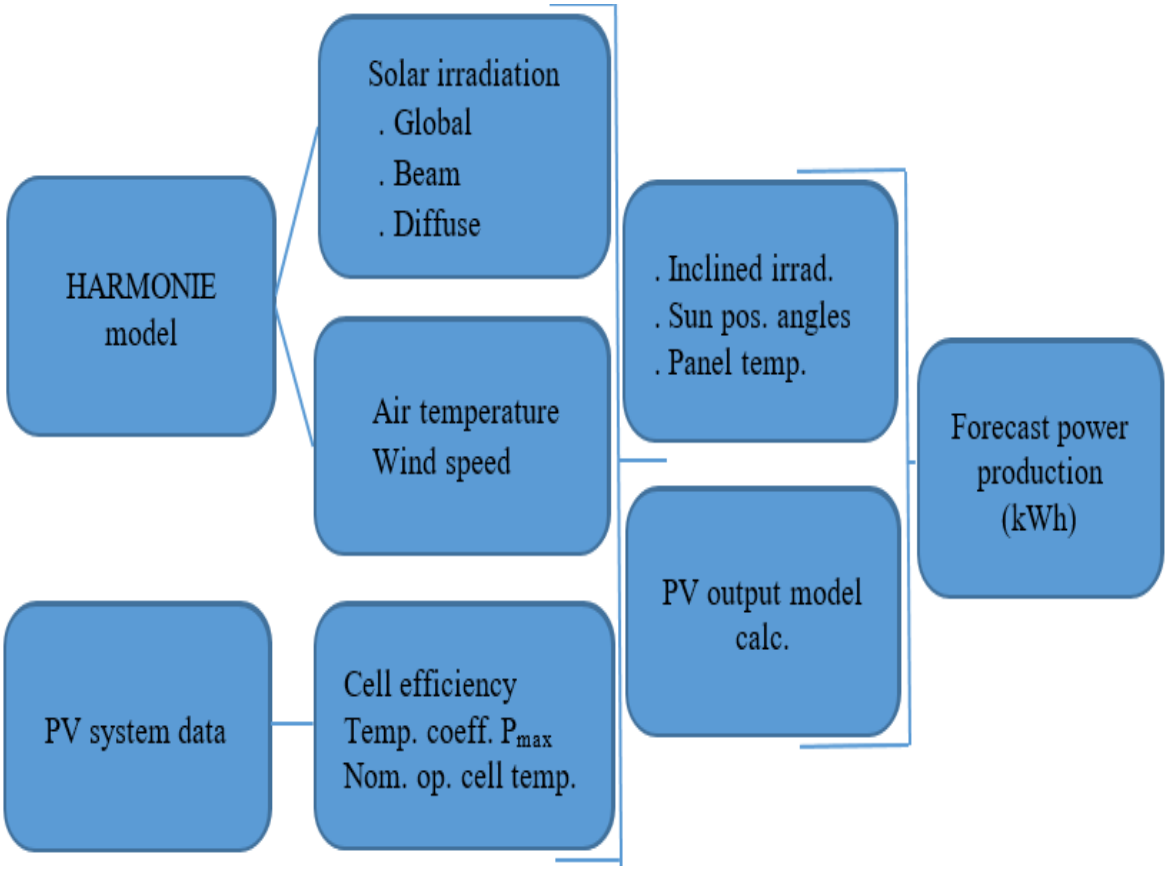

Figure 3: Methods of forecasting solar power production.

3.1. Observation on input variables for the PV power forecasting model

Typically, the accurate total solar irradiation data is used as an input parameter to derive the estimated power output. In addition, as mentioned in Section 3, the estimated power output is subject to the weather forecast and environmental factors ranging from solar irradiation, cloud cover, wind speed, relative humidity and air temperature. Similarly, the efficiency of the panels as well as their angle need to be considered. All these factors are pivotal in choosing the input variables for a prediction model (HARMONIE-AROME, 2011).

Figures 4 and 5 depicts solar irradiation on horizontal surface for seven days in May 2016 (May 21st – May 27th) and seven days in August 2016 and part of September 2016 (August 27th – September 2nd) respectively. Figure 6 represents the local weather variables precisely the air temperature and wind speed in Lappeenranta as generated by the HARMONIE model.

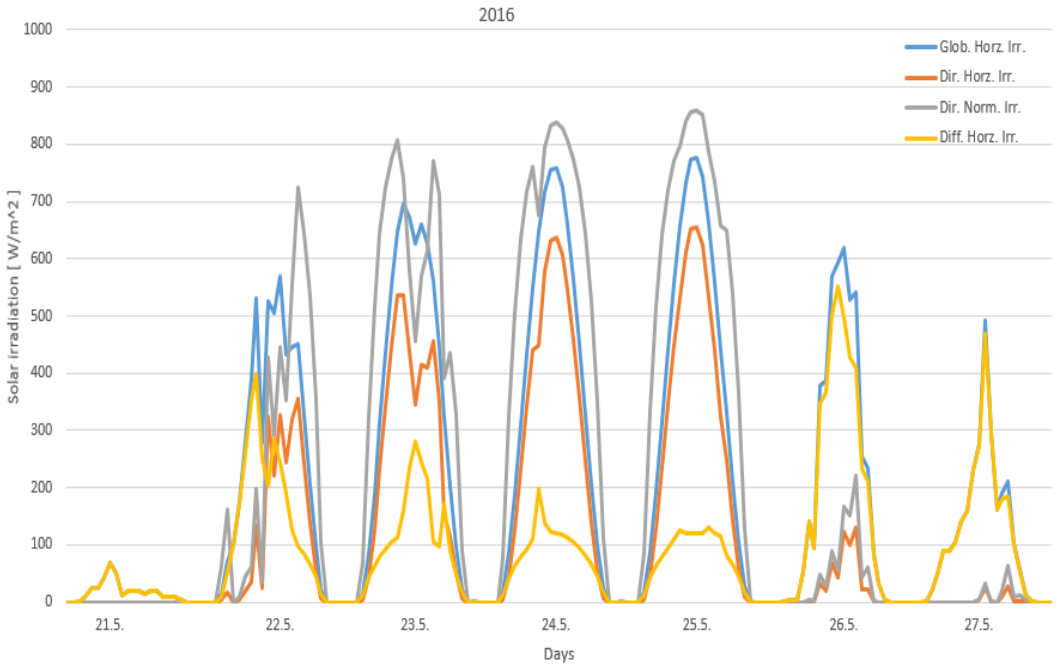

Figure 4: Solar irradiation on horizontal surface in Lappeenranta (21st – 27th May).

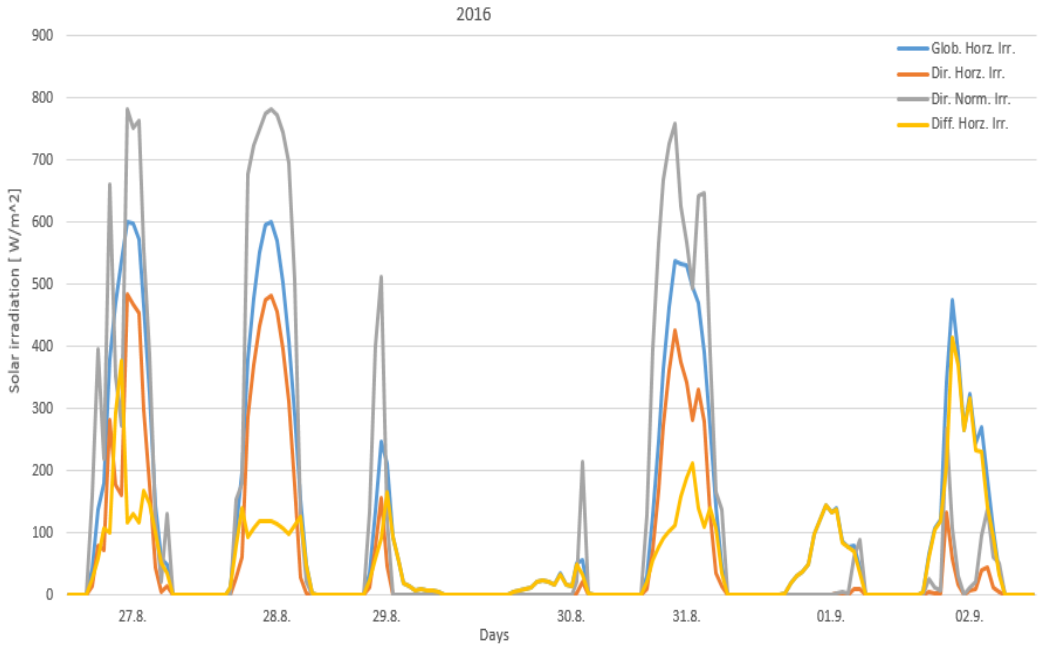

Figure 5: Solar irradiation on horizontal surface in Lappeenranta (27th Aug.– 02nd Sept. 2016).

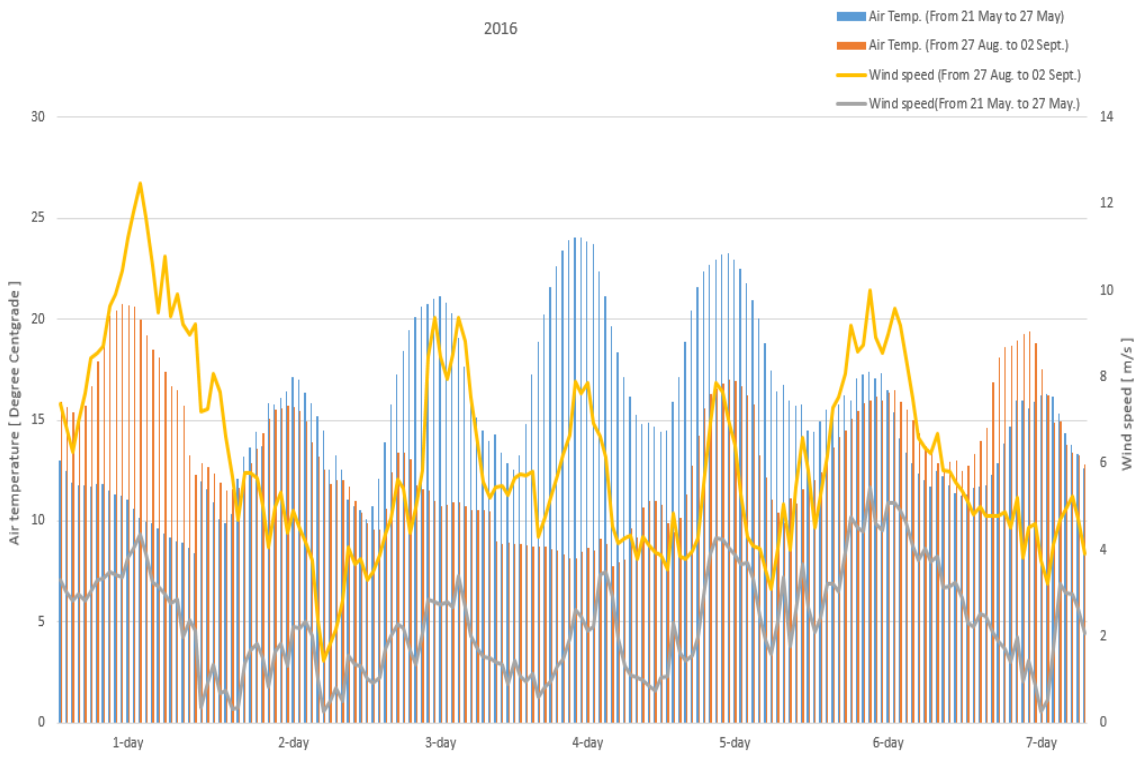

Figure 6: Air temperature and wind speed in Lappeenranta.

To facilitate the computation of the forecasted power output, various models were used with the weather conditions, particularly air temperature, solar irradiation, and wind speed as the input parameters. On the same note, solar panel characteristics: manufacturer's specification and system specifications to be exact, were used as input parameters in these models. Typically, this computation is well illustrated in Figure 3. As such, the following section puts the models and their components into perspective.

3.2. Solar geometry and irradiation components

According to Benford & Bock (1938), The geometric relation between any surface moving relative to the earth at any time (like the surface is fixed or moving relative to the earth) and incoming of solar irradiation is the position of the sun relative to the surface, it can be described with some angles Benford & Bock, (1938). The angles are shown in Figure 7.

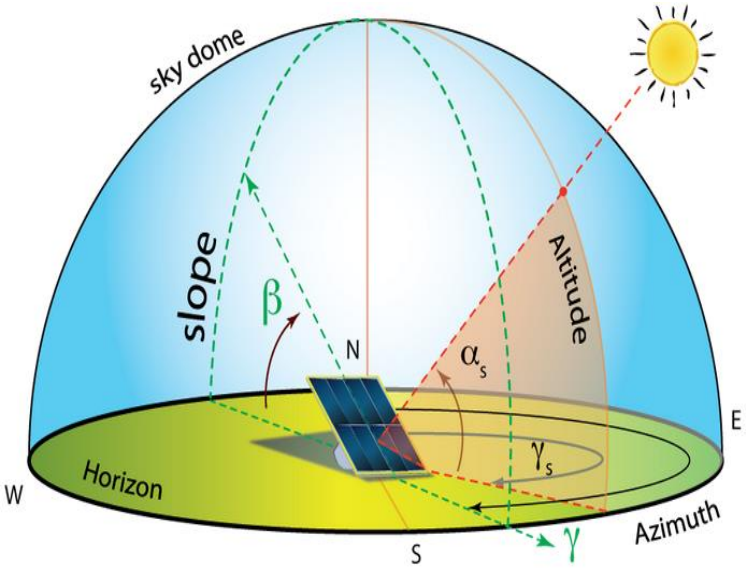

Figure 7: Collector-sun orientation: azimuth (γ), collector tilt (β), solar altitude angle (α_s), solar azimuth angle (γ_s) (Brownson, 2016).

3.2.1. Solar altitude (referred to as elevation) angle

Scharmer et al, (2000) defines solar altitude as the angle between the line of incoming sun rays and horizontal surface as shown in Figure 7. This solar altitude can be represented as shown in Eq. (1) (Scharmer et al, 2000).

$$\alpha_s = \sin^{-1}[\sin(\phi)\sin(\delta) + \cos(\phi)\cos(\delta)\cos(\omega)], \quad (1)$$

where α_s the solar altitude angle, ϕ the latitude angle and δ the declination angle also presented in Eq. (5), whereas ω the hour angle also presented in Eq. (11).

3.2.2. Zenith angle

According to Duffie and Beckman (2013), zenith angle can be defined as the angle between the line of the incoming sun and the vertical line. In other words, it is the angle of incidence of beam irradiation on a horizontal surface. The zenith angle can be described using Eq. (2) (Duffie & Beckman, 2013, p. 15).

$$\cos(\theta_z) = \cos(\phi)\cos(\delta)\cos(\omega) + \sin(\phi)\sin(\delta), \quad (2)$$

where θ_z is zenith angle.

3.2.3. Solar azimuth angle

Scharmer et al, (2000) describe the solar azimuth angle as one giving the direction of the sun. They define it as the angle between the vertical plane containing the direction of the sun and the vertical plane running from South to North through a horizontal surface. Figure 7 depicts the solar azimuth angle whose value is positive when the sun is to the West of South-North meridian. As Scharmer et al, (2000) assert, the solar azimuth angle γ_s, is measured due from North in the Southern Hemisphere and due from South in the Northern Hemisphere. Therefore, in Lappeenranta we measure the azimuth angle due from North where the sun is in the Southern Hemisphere for fixed modules facing South direction. The angle can be represented as follows:

$$\cos(\gamma_s) = (-)\frac{\sin(\phi)\sin(\alpha_s) - \sin(\delta)}{\cos(\phi)\cos(\alpha_s)}, \tag{3}$$

where γ_s is the solar azimuth angle.

Gilbert (2004) defines the declination angle as the angle between the equator and the line drawn from the center of the Earth to the center of the sun. The angle varies due to the tilt of the earth on its axis and the rotation of the Earth around the Sun which covers 365.25 days per one revolution. Given that the earth is about 149 million kilometers away from the sun, Gilbert 2004, defines a perihelion as a point when the earth is nearest to the sun at approximately 147 million kilometers while an aphelion as a point when the earth is about 152 million kilometers from the sun. The change in a distance can be determined by Eq. (4).

$$d = 1.5\ x\ 10^8\ \left\{1 +\ 0.017\ \sin\left[\frac{360(n-93)}{365}\right]\right\}, \tag{4}$$

where n is the day number of the with January 1 as the day 1 and December 31 being day number 365) (Gilbert, 2004, p. 390).

In Figure 8, the line formed by the earth rotating around the sun is explained ecliptic plane. On 21st March and 21st September, the line between the sun and the earth passes through the equator and we have 12 hours in daytime and 12 hours at night which is an *equinox*, (when

day and night are of equal length) while in 21st December, is a winter time called *solstice* in the Northern Hemisphere. In the North Pole, the angle is highest from the sun at 23.45° (Gilbert, 2004, p. 391).

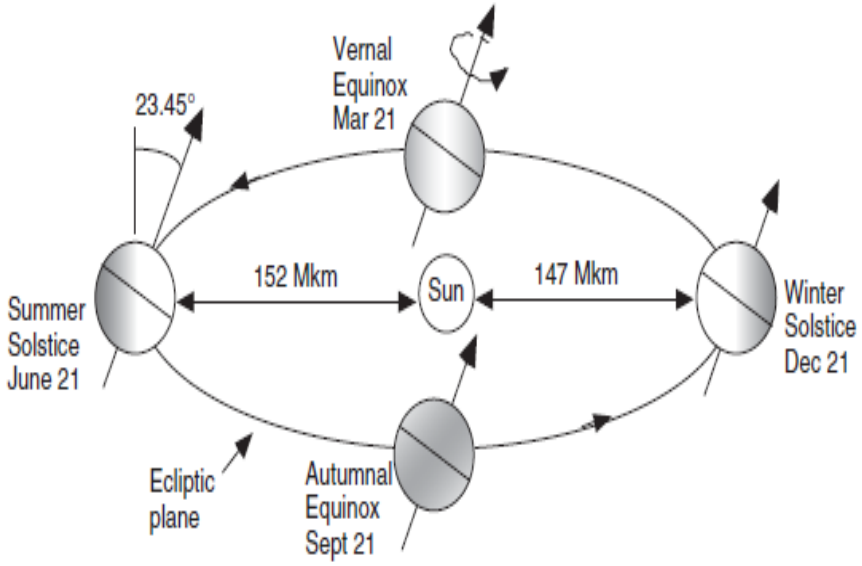

Figure 8: The angle of the rotational of the earth on the axis with ecliptic plane, (Gilbert, 2004).

As we know, the sun starts to rise from the east and set in the west direction and the sun is at the highest point during the middle of the day. It is important to estimate the exact position of the sun in a day in the year. In the case of solar PV system, we should understand the angle of the sun, which can optimize the maximum power output. On 21st June (summer solstice) the sun is at the highest point making an angle of 23.45° at the equator of the earth. Hence, the sun is above the Tropical of Cancer at the latitude 23.45°. On December 21, the angle is negative 23.45° known as the Tropic of Capricorn. As shown in Figure 9, the angle created between the equator line and the sun line is defined as solar declination angle δ. It is reached at the highest degree between $\pm$ 23.45°. Based on our calculations, we assume total number of 365-days in a year and which set spring equinox in the day n = 81 as a preferred good approximation (Gilbert, 2004, p. 392).

$$\delta = 23.45 \sin\left[\frac{360}{365}(n - 81)\right], \tag{5}$$

where δ is the solar declination angle in (degree) and n the number of the day.

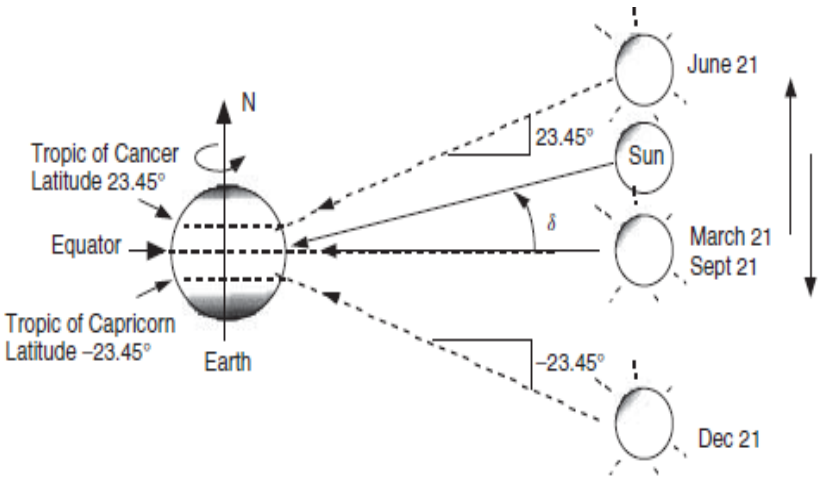

Figure 9: An alternative view with fixed earth and a sun that moves up and down. (Gilbert, 2004, p. 392).

3.2.4. Solar time

According to Rekioua & Matagne (2012), considering the Civil Time (CT) in hours is the initial stage towards finding Hour Angle (HA). A Greenwich Mean Time (GMT) or Universal Time (UT), can be found by subtracting the Time Difference (TD), (this time difference depends on a seasonal change of some countries) (Rekioua & Matagne, 2012, p. 37) as indicated in Eq. (6) below.

$$\mathrm{UT} = \mathrm{CT} - \mathrm{TD}, \tag{6}$$

where UT is the Universal Time, CT the Critical Time and TD the Time Difference.

We use the longitude for Lappeenranta at 28°.091´E to obtain Mean Solar Time (MST) by the Eq. (7) (Rekioua & Matagne, 2012, p. 37).

$$\mathrm{MST} = \mathrm{UT} + (long/15)\,, \tag{7}$$

Then, the Real Solar Time (RST) can be calculated by using Eq. (8) (Rekioua & Matagne, 2012, p. 37).

$$\mathrm{RST} = \mathrm{MST} + Et\,, \tag{8}$$

where Et is the equation of time, which can be found from the Earth rotation around the sun which is not uniform. The equation of the time is obtained from Eq. (9) as shown below.

$$\begin{aligned} Et(N) &= 0.000075 + 0.001868\cos(B) - 0.032077\sin(B) \\ &-0.014615\cos(2B) - 0.04089\sin(2B) \end{aligned} \tag{9}$$

where

$$B = \frac{2\pi(N-81)}{365}, \tag{10}$$

Finally, the Hour Angle (HA) can be obtained as indicated by the following Eq. (11).

$$\mathrm{HA}\ (\omega) = \frac{\pi}{12}(\mathrm{RST} - 12) \tag{11}$$

In this thesis the computation of the forecasting power output, we need to propagate these forecasting solar irradiation components and use these data to estimate the total solar irradiation on a tilted surface. The total solar irradiation dependency of the sun position angle on a time, for an example in Figure 10, the results have gotten the sun position angles estimation on 21st May 2016 in Lappeenranta.

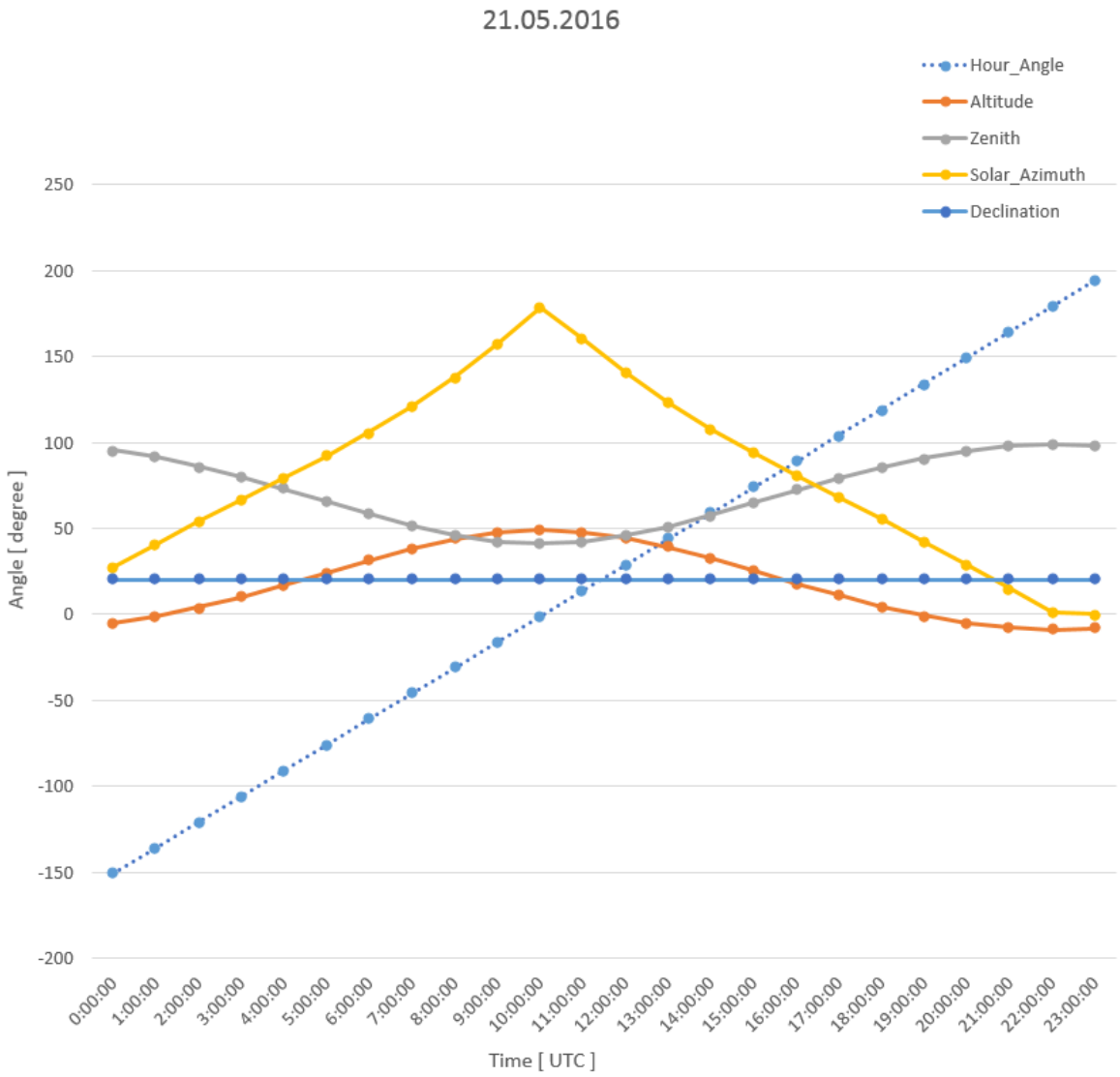

Figure 10: The sun position angles estimation on 21st May 2016 in Lappeenranta.

3.2.5. Total solar irradiation on a tilted surface

To estimate the solar irradiation on tilted surface, we need to know altitude angle and azimuth angle of the sun accurately. The solar irradiation on tilted surface is calculated by using these angles depending on the geographical coordinates of the location area. These angles with irradiation components provides the amount of solar irradiation on tilted PV panel, the solar irradiation comes through the three components, which are beam (direct), diffuse and ground-reflected irradiation. These components are shown in Figure 11.

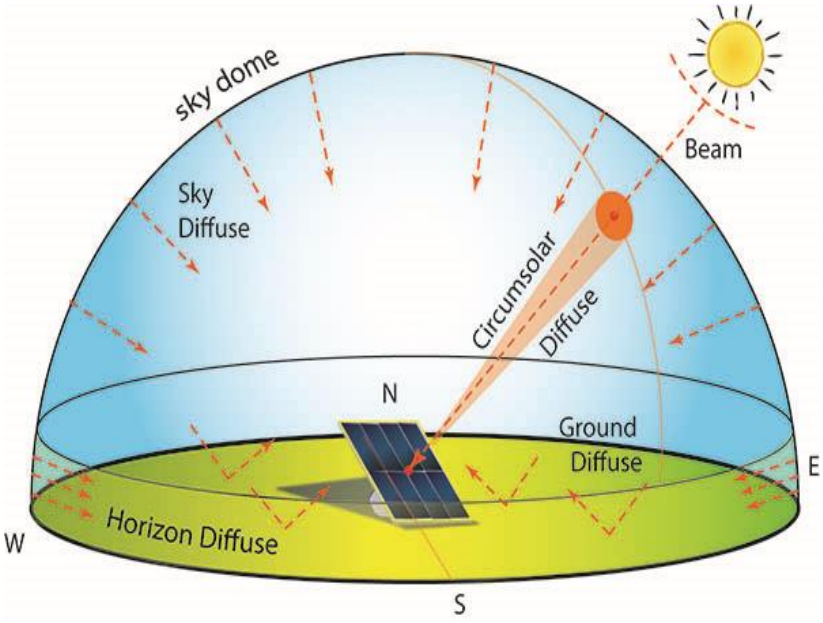

Figure 11: Diffuse, beam (direct) and ground-reflected irradiation on a tilted Surface (Brownson, 2016).

The total solar irradiation needs to be reflected on PV panel. It is very important to use these components to estimate output power production. The reflection of ground surface depends on the location area where the panels are installed. For satisfactory results calculation of diffuse and beam irradiation, the model was introduced and published by HAY and McKAY (1985) which proposed the circumsolar diffuse and horizon-brightening components on the tilted surface (HAY & McKAY, 1985).

This model is called Hay-Davis-Klucher-Reindl (HDKR) model, which estimates the fraction of all circumsolar diffuse to be the same as the beam irradiation on a tilted surface. However, the model suggestion improved the horizon-brightening relevant diffuse part

Klucher (1979) and gives good output results using input data for example the hourly data or monthly data of diffuse, global, beam horizontal irradiation and solar geometry system.

The modeling calculation of total solar irradiation on tilted surface (I_T) described Eq. (12).

$$\underbrace{(I_b + I_d A_i) R_b}_{\text{=direct \& circumsolar diffuse}} + \underbrace{I_d (1 - A_i) \left(\frac{1 + \cos(\beta)}{2}\right) \left[1 + f \sin^3\left(\frac{\beta}{2}\right)\right]}_{\text{=diffuse sky \& horizon}} + \underbrace{I_g \rho_g \left(\frac{1 - \cos(\beta)}{2}\right)}_{\text{=ground reflected}}, \tag{12}$$

where the beam horizontal irradiation I_b, the diffuse horizontal irradiation I_d, the anisotropy index A_i, the tilt factor for the beam irradiation R_b, the global horizontal irradiation I_g, the ground reflected ρ_g, the panel tilt angle β, and the modulating factor f.
The anisotropy index described by given Eq. (13) (Duffie & Beckman, 2013, p.92).

$$A_i = \frac{I_b}{I_0}, \tag{13}$$

where the extraterrestrial on horizontal irradiation I_0.
The modulating factor f can be considered for the cloudiness depending on the weather condition, it is described by the given Eq. (14) (Duffie & Beckman, 2013, p.92).

$$f = \sqrt{\frac{I_b}{I_g}}, \tag{14}$$

where I_g, is the global horizontal irradiation and I_b is the beam horizontal irradiation.
For the diffuse, ground-reflected and beam irradiation, the tilt factor R_b are changed as described by the Eq. (15) (Duffie & Beckman 2013, p.24).

$$R_b = \frac{\cos(\theta)}{\cos(\theta_z)}, \tag{15}$$

where the angle of the incidence between the beam and normal surface is θ and the zenith angle is θ_z.

3.2.5.1. Fixed modules

The fixed modules on a tilted surface can be used in different systems. This can be attributed to the fact that the fixed modules on a tilted surface is widely more accessible than other PV module systems. In order to obtain accurate output from the fixed module systems, a number of factors need to be considered among them being the angle of incidence. This has therefore motivated the use of fixed panels from LUT solar power plant in our study. In particular, the fixed modules are facing the south direction with the angle of incidence leading to the Northern Hemisphere (γ = 0°). The description can be well illustrated using the following Eq. (16) (Duffie & Beckman, 2013, p. 16).

$$\cos\theta = \cos(\phi - \beta)\cos(\delta)\cos(\omega) + \sin(\phi - \beta)\sin(\delta) \quad (16)$$

where θ is the angle of the incidence, β the panel tilt angle, ϕ the latitude, δ the declination angle, ω the hour angle and γ the surface azimuth angle.

3.3. Physical model for PV power generation

Photovoltaic (PV) panels are semiconductor materials, which converts solar irradiation intensity from the sun light into electrical energy in watts per meter square. The semiconductor materials produce electrical energy by photoelectric effect when the intensity of solar irradiation is available to the PV panel (Kleissl, 2013). There are types of PV panels were established based on single and multi-crystalline silicon, the most popular used such as polycrystalline thin-film materials such as cadmium telluride (CdTe) and copper indium gallium diselenide (CIGS), microcrystalline silicon, or amorphous silicon. Photovoltaic models type of multi-junction have reached the highest conversion efficiencies. In 2012, the world has recorded the efficiency for PV cell as 43.5% for GaInP/GasAs/GaLnNAs (Sb) shown in Appendix 2 (Kurtz, 2012). The specific information required for each PV technology to estimate solar output power, is the amount of spectral distribution of solar irradiation available on the PV panel. Figure 12 presents the spectral response depending on the PV cell materials

converted to solar electricity energy. The performance of PV panels depends on environmental conditions, for PV panels the standard rating based on reference test conditions consist of standards for spectrum distribution of solar irradiation (Myers, 2011).

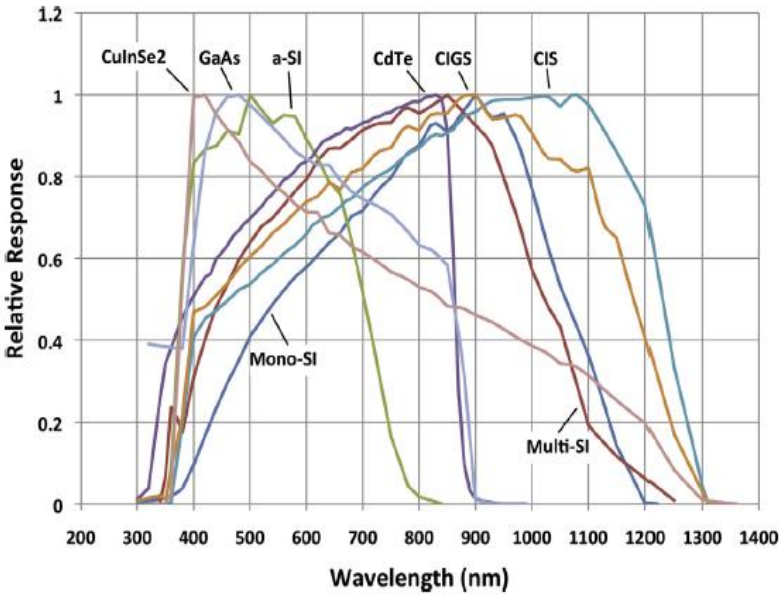

Figure 12: The spectral response depending on the PV cell materials, which convert the intensity of solar irradiation into electricity energy. (Courtesy of Chris Gueymard).

3.3.1. Photovoltaic electrical energy performance characteristics

A current and voltage (I-V) curve of PV panel represent its electrical energy conversion ability at the prevailing level intensity of solar irradiation and temperature. Theoretically, the curve describes the relation of current and voltage, in which the PV panel can be operated with the availability of solar irradiation and constant cell temperature. Figure 13 presents the characteristics of current and voltage (I-V), and power and voltage (P-V) curves shows the maximum power point (MPP) of the curve (Solmetric Corporation, 2011).

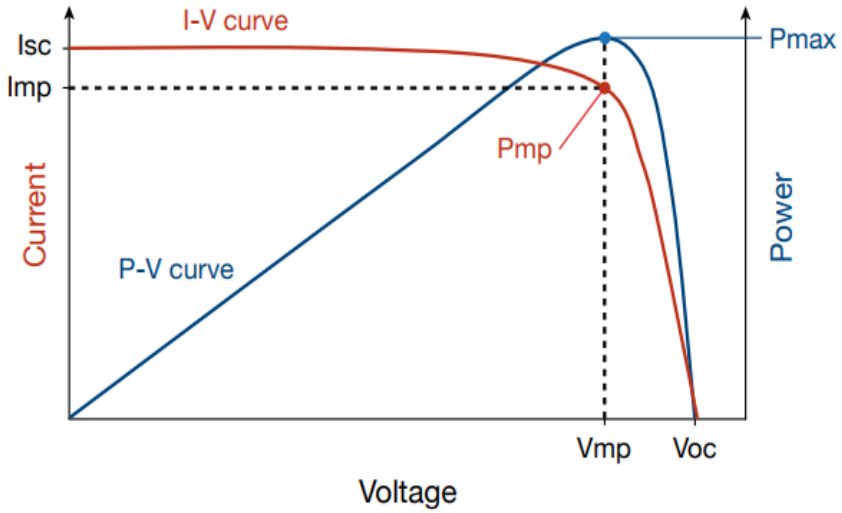

Figure 13: I-V and P-V curves are electrical energy characteristics of PV panel. The calculated P-V curve measured from I-V curve (Solmetric Corporation, 2011).

The I-V curve ranges from the short circuit (I_{sc}) at zero voltages to zero current at the open circuit voltage (V_{oc}). On the top of the I-V curve is the maximum power point (MPP), which the panel cells operate at maximum electrical power, this MPP is the given units of watt peak (W_p). At the low level of voltage V_{mp}, the electrical charge flowing to the exterior load is moderately independent of the output voltage. Close to the top of the curve at the MPP, the behavior can change, when the voltage increases, the more increasing percentage of charges combine again inside the solar cells (Solmetric Corporation, 2011).

The fill factor (FF) is an indicator performance of the PV panel. It is described as a rectangular shape of the I-V curve as shown in Figure 14. An ideal PV module technology generate rectangular I-V curve corresponding to the maximum power point with (I_{sc},V_{oc}), for the fill factor of 1. The fill factor computed by the ratio between two rectangular areas gives the following Eq. (17).

$$\frac{I_{mp}V_{mp}}{I_{sc}V_{oc}}, \tag{17}$$

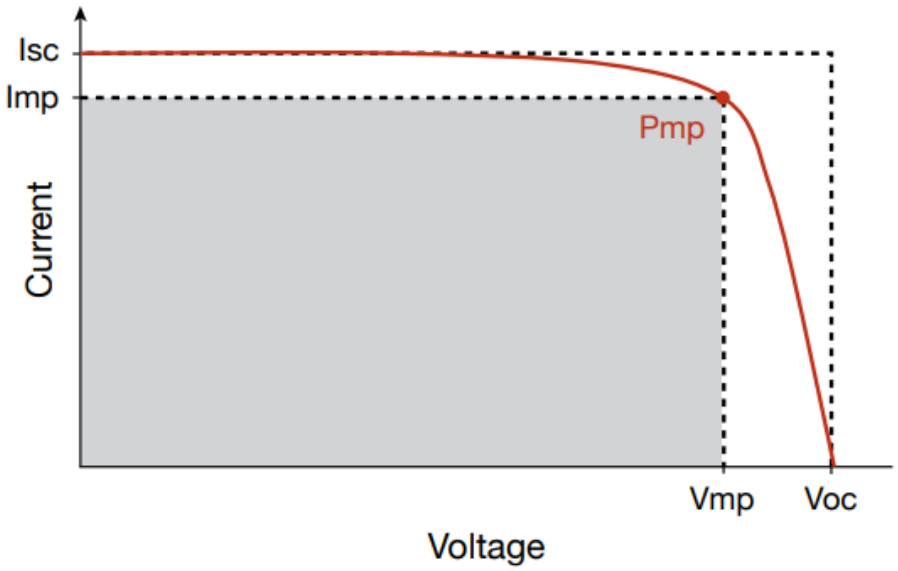

Figure 14: Observation area represents the fill factor from I-V curve (Solmetric Corporation, 2011).

The model number of the PV panels, should be related to the fill factors. The real magnitude of the fill factor depends on module design and technology. For example, the amorphous silicon module has lower fill factor than crystalline silicon module. Any of the losses can decrease the fill factor, which can also decrease the output power by decreasing V_{mp} and/or I_{mp}. Figure 15 represents the losses such as series losses, shunt losses and mismatch losses shown in the I-V curve. These losses reduce the height of the I-V curve by allowing a smaller amount of solar irradiation to reach on the cells panels or shading due to dust (Solmetric Corporation, 2011).

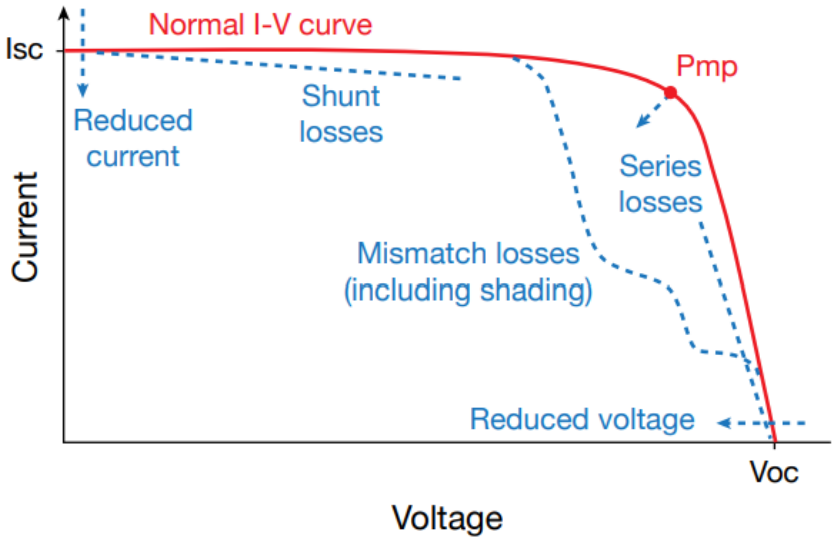

Figure 15: Types of losses as source decreases of PV panel power output (Solmetric Corporation, 2011).

3.3.2. Equivalent circuit for PV panel

The PV cell equivalent circuit shown in Figure 16. The current I_{ph} represents the cell photocurrent. The R_s and R_{sh} are series and shunt of the cell panel, respectively. The value of series resistance R_s is very small and the value of shunt R_{sh} resistance is very large, as a consequence, R_s may be neglected (Pandiarajan & Muth, 2011). Basically, the PV panel created by group of cells in larger units, which are connected in parallel or series to create a PV array used to produce electrical energy systems. This type of equivalent circuit is shown in Figures 16 and 17 present the equivalent circuit in solar array.

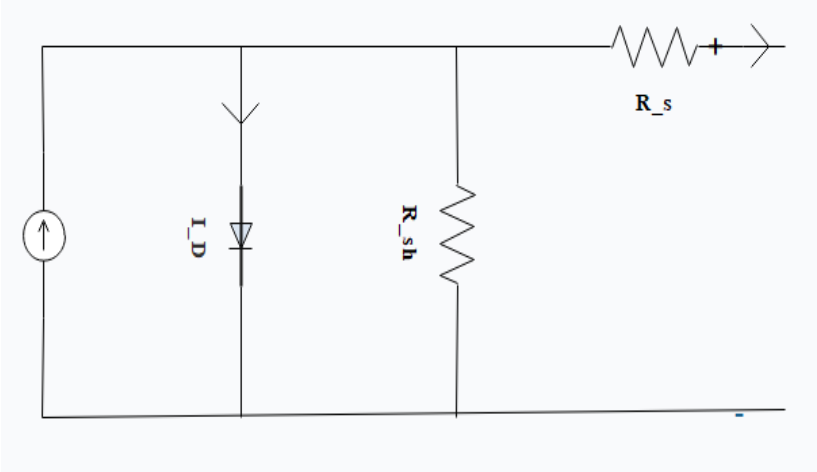

Figure 16: Equivalent circuit of PV cell, with series and parallel resistances.

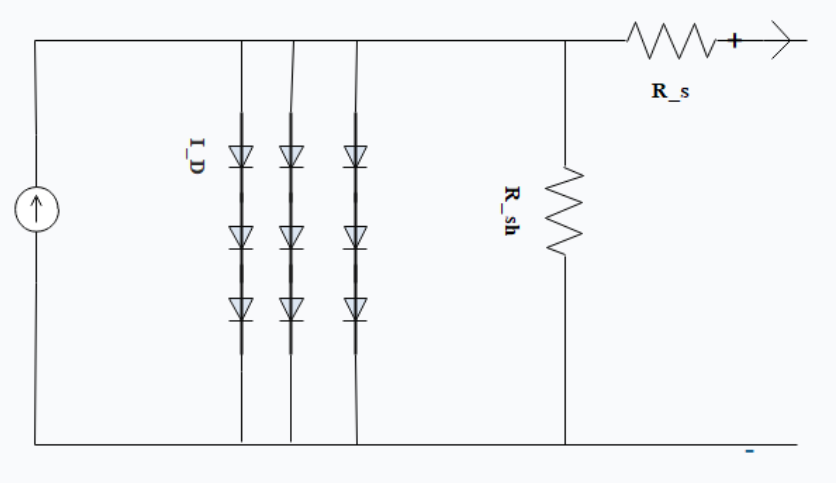

Figure 17: Equivalent circuit of solar array.

3.3.3. PV panel operating temperature

The panel cells operating temperature T_c is a major factor affecting the performance of PV power output system. There are three main parameters affecting the operating temperature: the air temperature T_a, total solar irradiation I_T, and wind speed v_f. However, there are other constant factors depending on the panel manufacturer specifications such as a heat exchange coefficient U_{PV}, transmittance absorptance product $\tau.\alpha$, PV panel efficiency η_{PV}, standard testing temperature T_{STC}, and temperature coefficient of maximal power under standard test conditions β_{STC} (Mattei et al., 2006). These panel performance parameters are tested at nominal operating cell temperature (NOCT). The nominal parameters for the PV panel used in this thesis is shown in Appendix 1.

There are several models for evaluating operating PV panel cells temperatures (Markvart, 2000), (Skoplaki et al., 2008), (Koehl et al., 2011), and (Kurtz et al., 2009). However, the model selected for this thesis is the one proposed by Mattei et al. (2006), shown in Eq. (18). This model is preferred because it has been evaluated using numerical weather prediction (NWP) and found to perform slightly better than the rest, according to the data from European Centre for Medium Range Weather Forecast (ECMWF) (Schwingshackl et al., 2013).

$$T_c = \frac{U_{PV}T_a + I_T[\tau.\alpha - \eta_{STC}(1 - \beta_{STC}T_{STC})]}{U_{PV} + \beta_{STC}\eta_{PV}I_T}, \quad (18)$$

where I_T is the total solar irradiation, the input parameters T_{STC}, η_{STC} and β_{STC} are efficiency and temperature coefficient respectively of maximal power under standard test conditions

(STC), $(\tau.\alpha) = 0.81$, v_w the local wind speed close to the panel, where v_f is the wind speed measured 10 meters above the ground. For transformation of two different wind speeds:

$$v_w = 0.68v_f - 0.5\,, \tag{19}$$

where the heat exchange coefficient is evaluated as a function of wind speed in Eq. (20), so that.

$$U_{PV} = 26.6 + 2.3v_w\,, \tag{20}$$

where U_{PV} is the heat exchange coefficient for the total surface of the panel calculated by (Mattei et al., 2006). The panel cells operating temperature is sensitive to the prevailing weather conditions mainly air temperature.

Figure 18. The relationship between air and panel operating temperature dependency of input variables such solar irradiation, air temperature, wind speed and panel setting on tilted at 15°. These variables input used from forecasted model output. As we can see the panel temperature rises due to increasing of solar irradiation at 13:00 solar noon, this is because the solar irradiation absorbed by PV panel cells and contribute the increases of panel temperature also as a result decreasing the power output of PV system (Schwingshackl et al., 2013). The use of wind speed considered as cooling effect on PV cells temperature, during the generated of PV cells, the heat removed from absorbed PV cells then operates at low temperature and increasing of power output with the decreases of the temperature. For instance, with polycrystalline silicon (p-Si) decreases approximately −0.44%/°C, when the temperature is higher than 25°C (Schwingshackl et al., 2013).

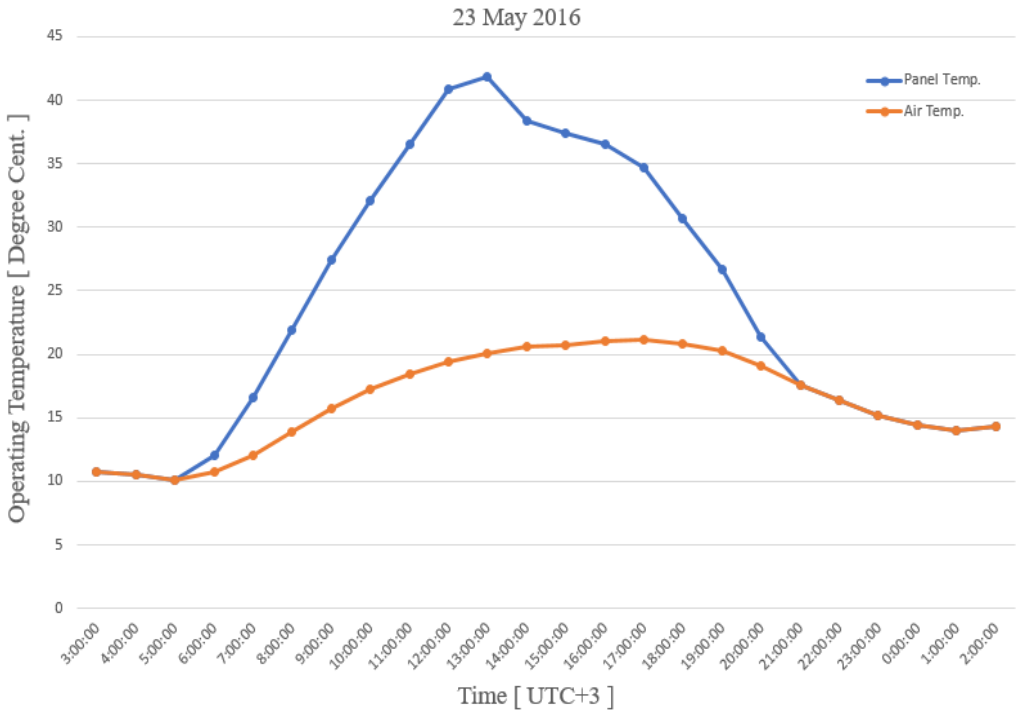

Figure 18: Relationship between air and panel operating temperature captured on 23rd May 2016.

The estimated PV power output as a function of cell temperature represented by Eq. (21).

$$P_{PV} = \eta_{PV} A I_T [1 - \beta_{STC}(T_c - T_{STC})], \quad (21)$$

where P_{PV} the total power estimated, η_{PV} the panel efficiency, T_c the panel operating temperature , A the total area of the PV panel, β_{STC} the temperature coefficient of maximal power of the panel cells at (STC), for polycrystalline silicon (Pc-Si) approximately −0.44%/°C, T_{STC} the ambient temperature at (STC), which given at 25°C and I_T the total solar irradiation on tilted surface.

4. Results

This section presents the results of output power between forecast and real power production. The real power is measured from the PV system installed at LUT in Lappeenranta region. As referred in Section (3), the input variables such as forecast solar irradiation and local weather variables such as wind speed, temperature, are obtained from the HARMONIE model. The computation of the forecasted power output needed to factor the number of solar panels in the solar production plant. The panels constituting the PV system were mounted at 15° tilt angle facing south direction. The total maximum peak power and the efficiency per each panel is 5.06 kW_p and 14.1% of 230 W_p respectively. The panels were using polycrystalline silicon (p-Si) materials (Tianwei TWY230P60-FA2).

Excel software was used for computation of the forecasted power output which was done using the models discussed in Section (3). The calculation of the estimated power output also factored the efficiency of the inverter (97 %).

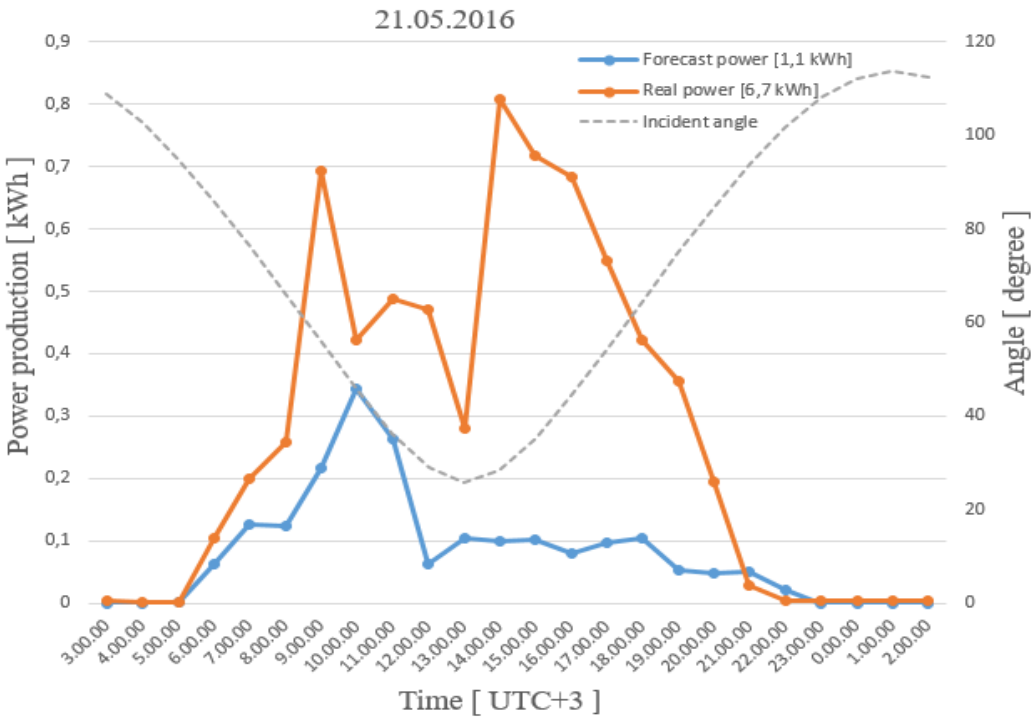

Figure 19: Forecast and real power production on fixed PV system on 21st May.

As indicated in Figure 19, the peak from real power is higher than the forecasted power. This can be attributed to the cloud weather distribution, which appears to occupy the better part of the day from morning to evening. This is clearly depicted in Table 1. The cloud weather is a major impact of NWP model as it may influence the variability level of solar irradiation thus affecting the maximum power output. Moreover, the cloud weather might influence both the diffuse irradiation and the beam irradiation.

Table 1: Average local weather distribution on 21st May at Lappeenranta (FMI, 2016).

Date/Time	**Cloud coverage (%)**	**Humidity (%)**	**Rain (mm)**
21.05.2016			
00:00	38	69	0.0
03:00	85	82	0.2
06:00	100 (mostly cloudy)	90	0.7 (light rain)
09:00	100	94	0.8
12:00	100	95	0.0
15:00	100	95	0.0
18:00	100	96	0.0
21:00	100	97	0.0

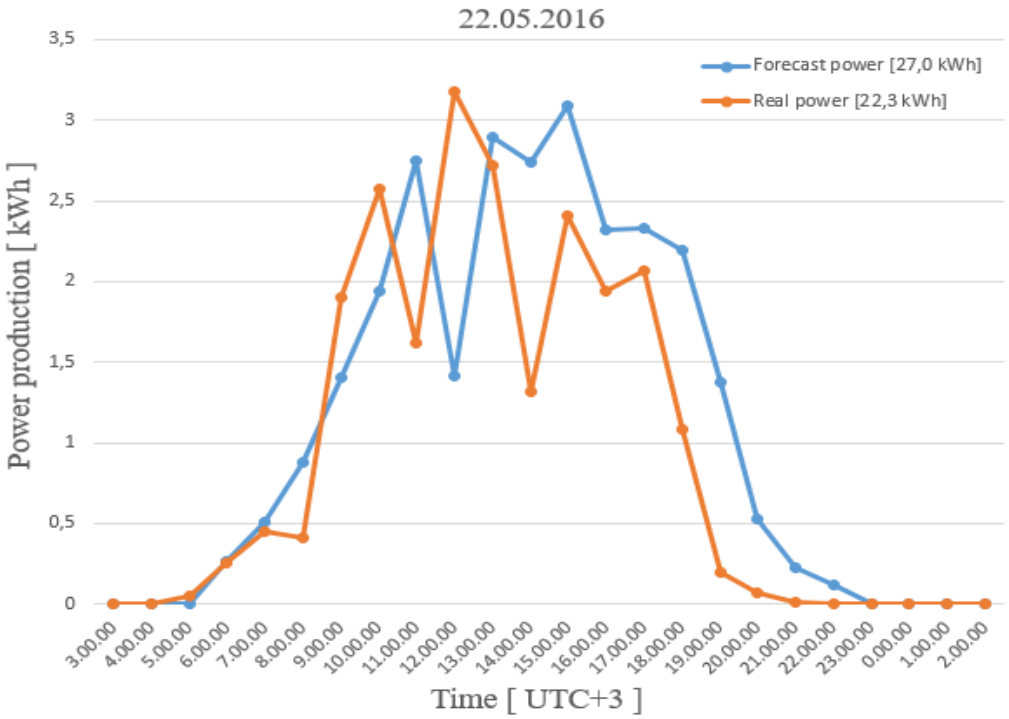

Figure 20: Forecast and real power production on fixed PV system on 22nd May.

In Figure 20, forecast and real power reaches to the maximum peak and the power are unstable between 10:00 and 18:00. As illustrated from the Figure 20, there was less cloud cover of about 45% as well as no rainfall on this day.

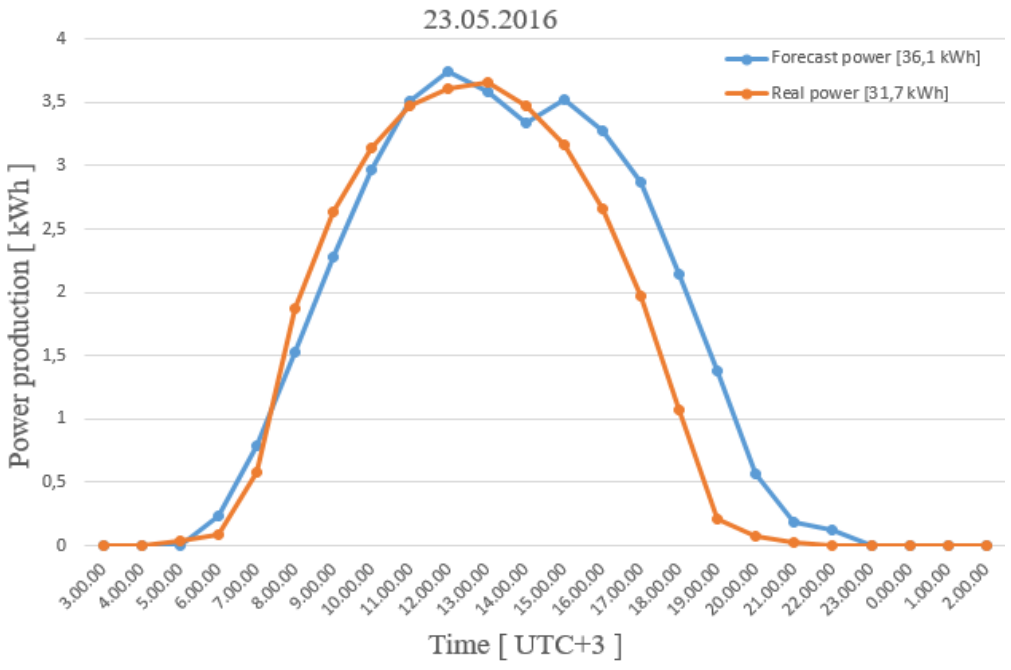

Figure 21: Forecast and real power production on fixed PV system on 23rd May.

As indicated in the Figure 21, there was a linear relationship between the forecasted power and real power especially in the morning from 05:00 – 13:00. During this day, the cloud cover ranged between 4% and 9%. The small deviation as observed from the Figure 21 could be attributed to the increasing cloud intensity especially from 15:00. The maximum power generation depends on the intensity of cloud covering the sky.

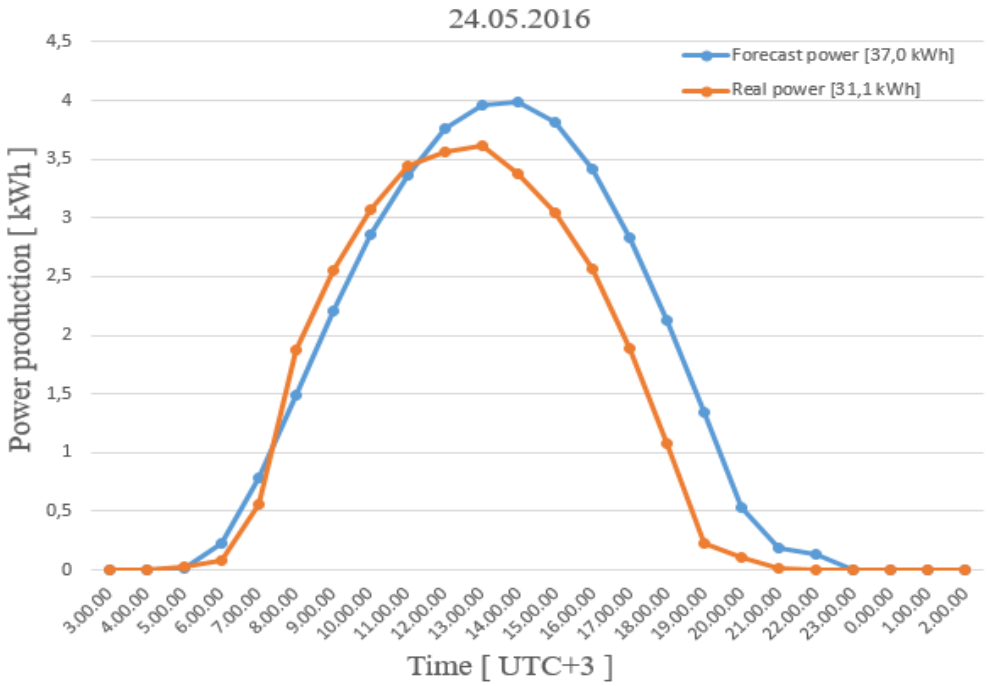

Figure 22: Forecast and real power production on fixed PV system on 24th May.

As shown in Figure 22, the curves representing both the real and forecast power are smooth and stable. This can be attributed to the fact that the day is a clear one owing to the little cloudy as captured in Table 2. A similar observation is made on the following day 25/05/2016 as illustrated in the Figure 23. However, the minor observation can be attributed to the change in the inverter efficiency arising from the humidity weather as well as dust on the solar panels.

Table 2: Average local weather distribution on 24th May at Lappeenranta (FMI, 2016).

Date/Time	Cloud coverage (%)	Humidity (%)	Rain (mm)
24.05.2016			
00:00	6	88	0.0
03:00	5	84	0.0
06:00	5	70	0.0
09:00	6	53	0.0
12:00	8	44	0.0
15:00	10	44	0.0
18:00	7	50	0.0
21:00	5	60	0.0

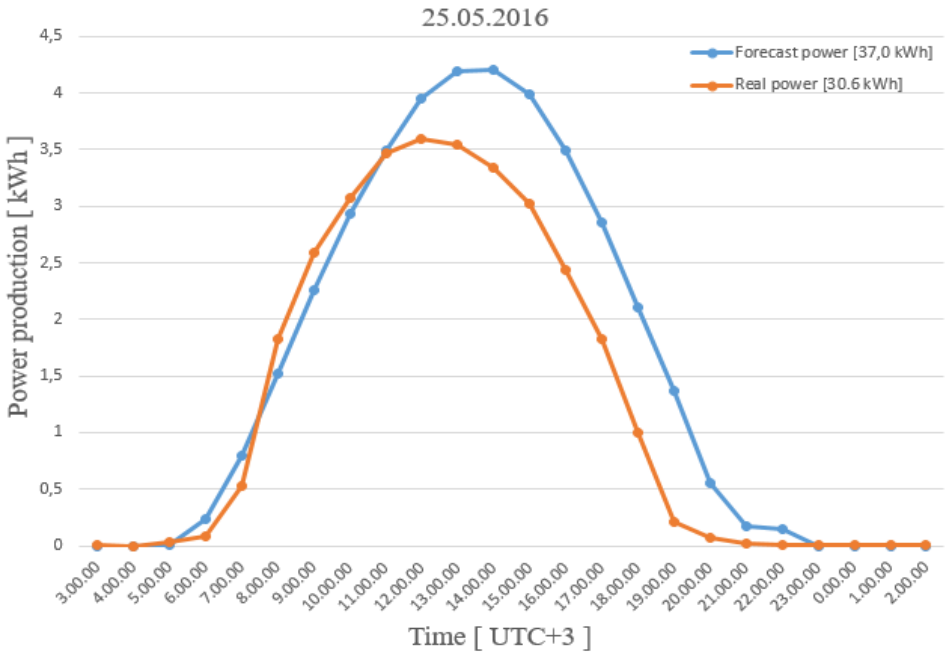

Figure 23: Forecast and real power production on fixed PV system on 25th May.

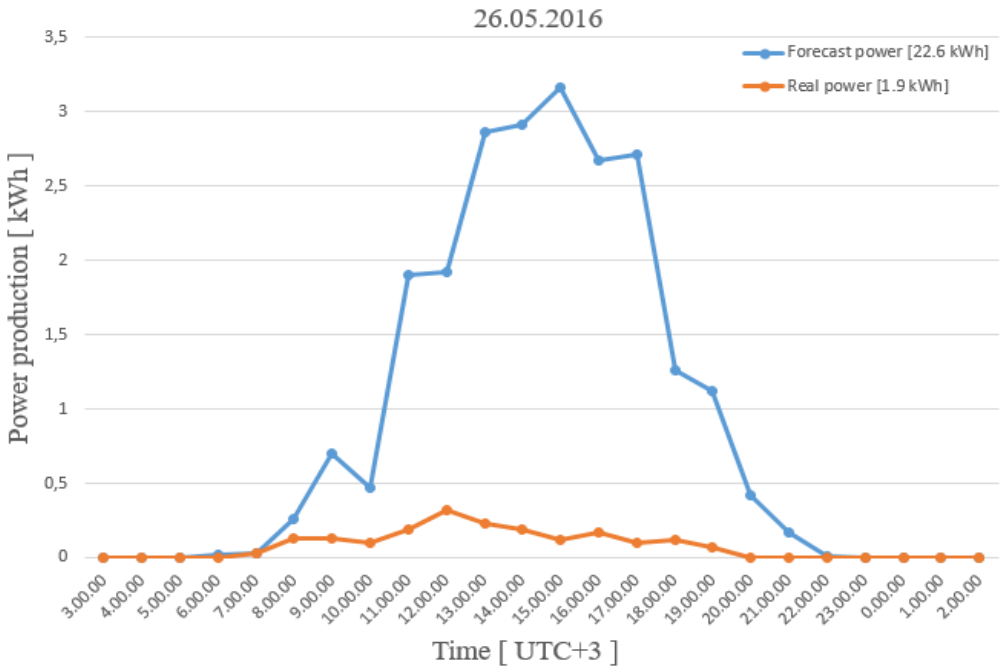

Figure 24: Forecast and real power production on fixed PV system on 26th May.

The forecast power as shown in Figure 24 is higher than the real power. The light rainfall and the rapid rise in cloud intensity as illustrated in Table 3 appears to affect the actual production of solar thus influencing its output from the PV system.

Table 3: Average local weather distribution on 26th May at Lappeenranta (FMI, 2016).

Date/Time	**Cloud coverage (%)**	**Humidity (%)**	**Rain (mm)**
26.05.2016			
00:00	66	88	0.1
03:00	82	96	0.4
06:00	100	95	0.7 (light rain)
09:00	95	90	0.5
12:00	76 (partly cloudy)	82	0.7
15:00	60	81	1.6 (chance rain)
18:00	72	86	1.0
21:00	98	90	0.1

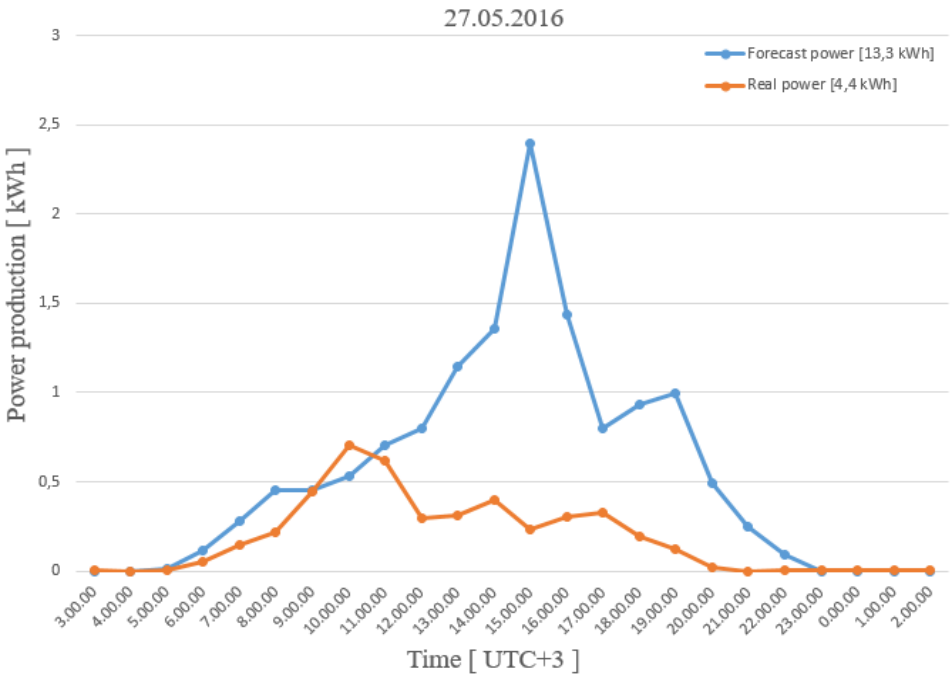

Figure 25: Forecast and real power production on fixed PV system on 27th May.

As Figure 25 illustrates, the power forecasting on 27th May is much higher than the real power. On this day the cloud distribution appears to be less than 60% between 09:00 and 21:00. As shown on the graph, the peak forecast power is recorded at 15:00, with the real power appearing to be significantly steady, though low as compared to the forecast power.

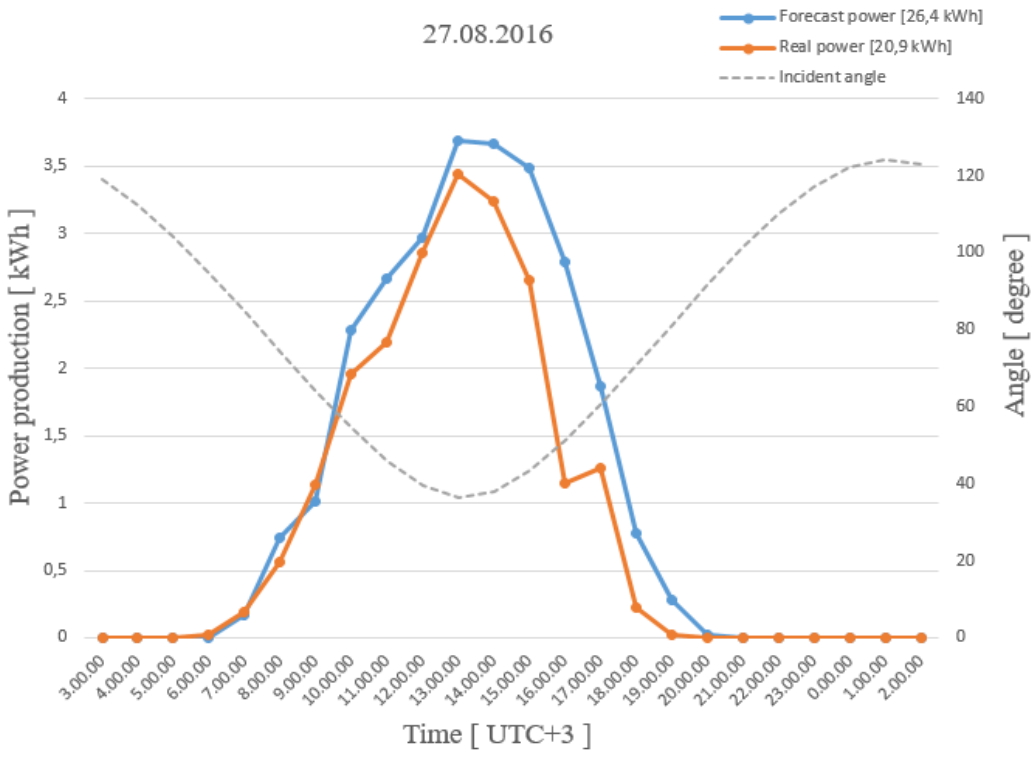

Figure 26: Forecast and real power production on fixed PV system in 27th August.

As illustrated in Figure 26, there appears to be a direct proportion between the real power and the forecasted power during the entire day. This is as a result of lower cloud intensity with the clear clouds at noon as indicated in Table 4, which appears not to affect the power output.

Table 4: Average local weather distribution on 27th August at Lappeenranta (FMI, 2016).

Date/Time	Cloud coverage (%)	Humidity (%)	Rain (mm)
27.08.2016			
00:00	53	85	0.0
03:00	31	90	0.2
06:00	16	84	0.7
09:00	17	71	0.8
12:00	8 (clear)	53	0.0
15:00	13	50	0.0
18:00	48	53	0.0
21:00	73 (partly cloudy)	60	0.0

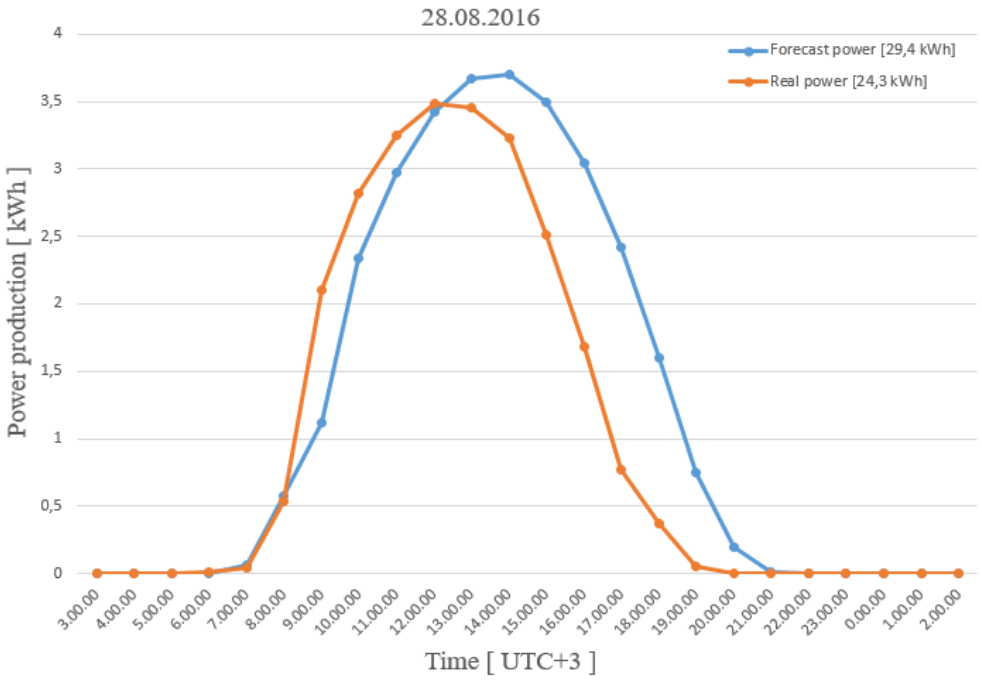

Figure 27: Forecast and real power production on fixed PV system in 28th August.

As indicated in Figure 27, the forecast and real power was relatively the same as indicated by the smooth curves. The highest peak of real power is observed at noon owing to typically cloudness day. However, there is a slight deviation of forecast power from the real power which can be associated with the change in inverter efficiency attributed to the dust on the panel surface.

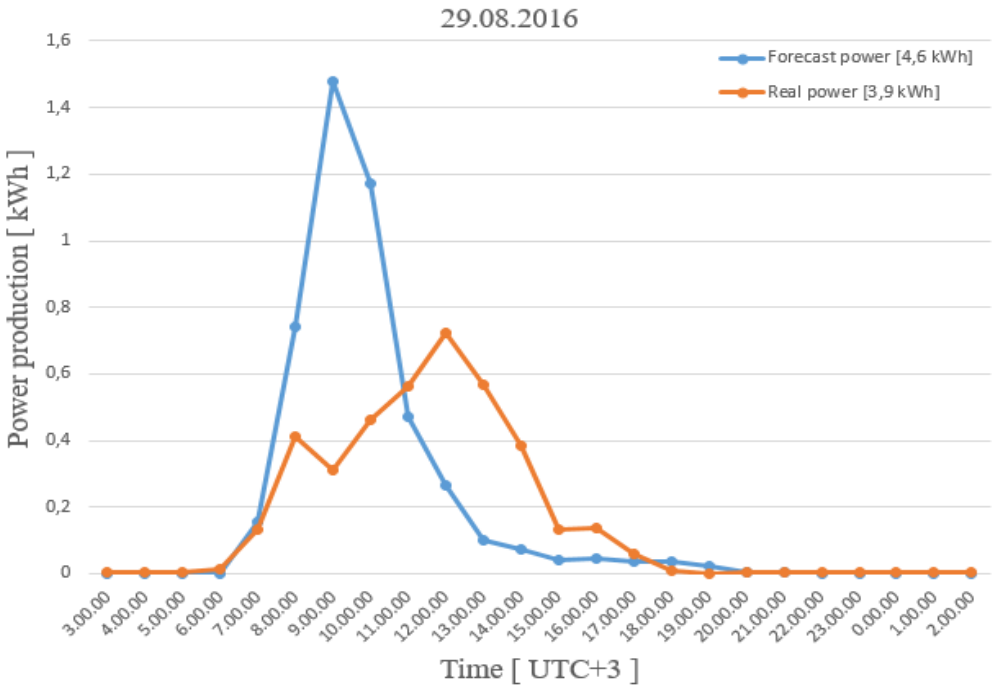

Figure 28: Forecast and real power production on fixed PV system in 29th August.

As shown in Figure 28, there is a decline in real power as the forecast power increases with peak forecast power being recorded at 09:00 on the 29th August. The falling of the rain and the cloud coverage could have contributed to the decline in the real power produced as indicated in Table 5. On the following day in Figure 29 the, peak of real power differs from forecast power, on this day there is no rain fall but there is maximum cloud cover especially between 15:00 and 21:00. The cloud shading could have also affected the intensity of the sun radiation reaching the surface of the panel thus affecting the production of the real power.

Table 5: Average local weather distribution on 29th August at Lappeenranta (FMI, 2016).

Date/Time	Cloud coverage (%)	Humidity (%)	Rain (mm)
29.08.2016			
00:00	70	63	0
03:00	36	69	0
06:00	47	77	0
09:00	80	82	0.5 (light rain)
12:00	94	91	4.3 (heavy rain)
15:00	100 (mostly cloudy)	94	9.8 (heavy rain)
18:00	100	95	5.8 (heavy rain)
21:00	100	96	0.9

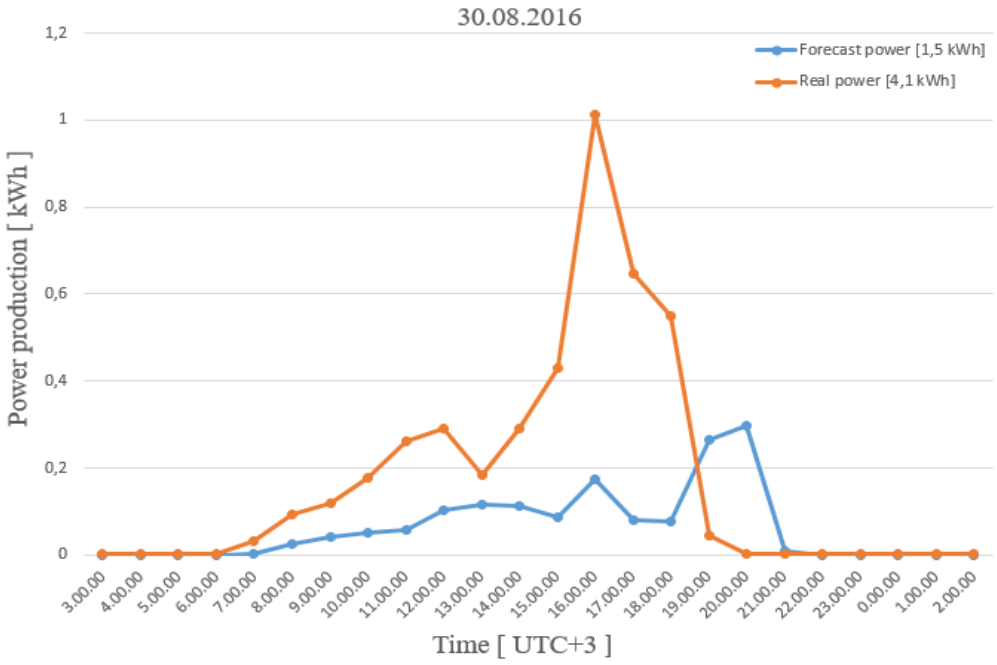

Figure 29: Forecast and real power production on fixed PV system in 30th August.

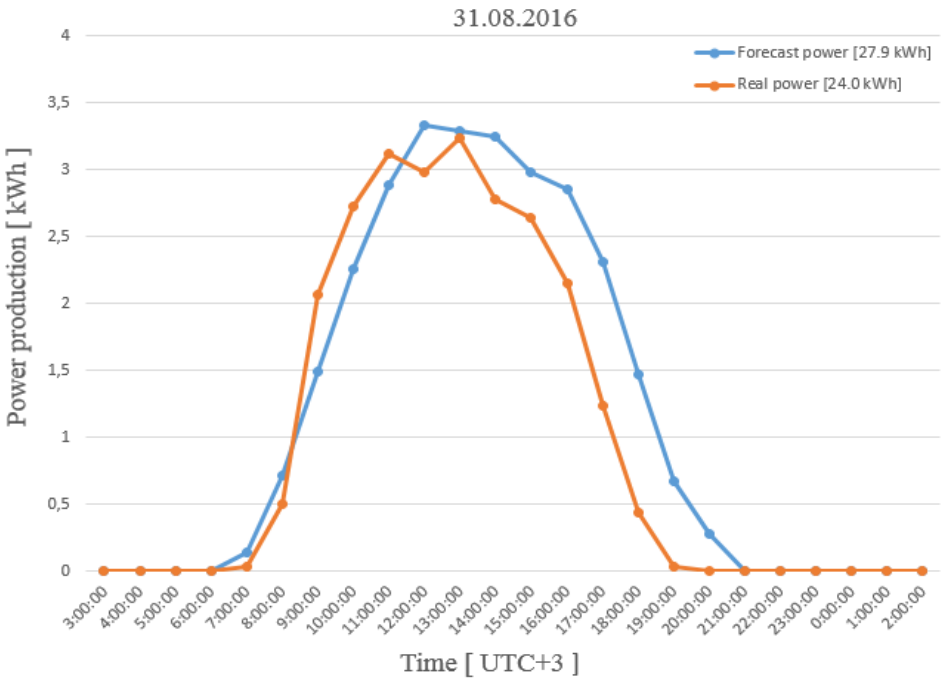

Figure 30: Forecast and real power production on fixed PV system in 31st August.

As noted from Figure 30, both the forecasted and the real power appears to vary proportionately with both appearing to coincide at 11:00. The cloud distribution on this day (31st August 2016) appears to be normal with it being clear at around noon.

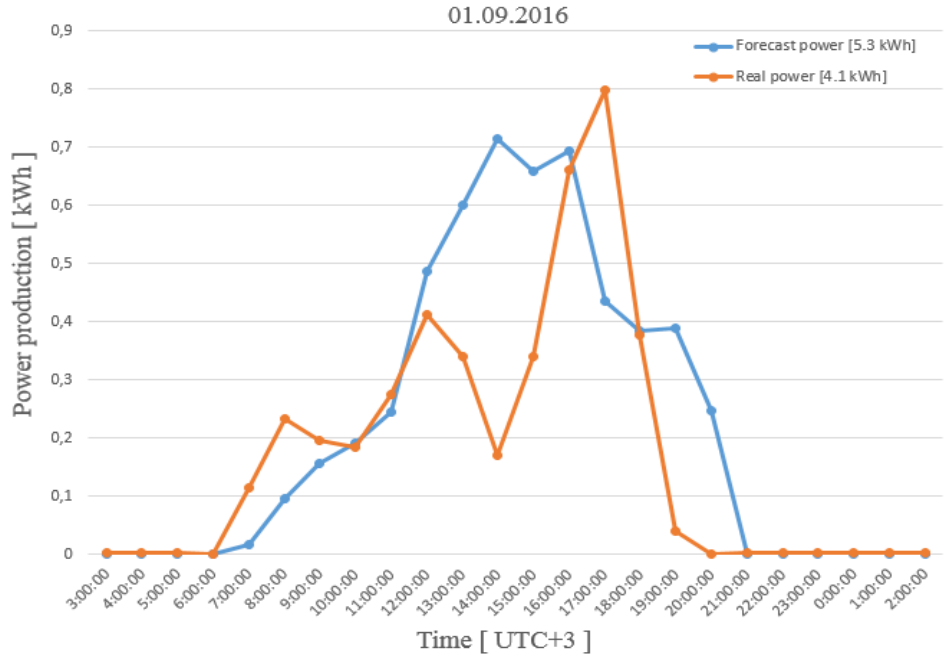

Figure 31: Forecast and real power production on fixed PV system in 01st September.

As observed from Figure 31, there is a great deviation between the forecast and real power which results to the fluctuation of the power output. This can be explained by the change of the cloud cover which appears to be increasing gradually as indicated in Table 6. As observed, the real power is typically low in the better part of the morning as a result of the cloud shadowing the surface of the panels thus reducing the amount of the solar irradiation reaching the surface of the panel. Also, this day is marked with humidity which when reaching its maximum level, affects the efficiency and the performance of the panel thus impacting the production of power output.

Table 6: Average local weather distribution on 01st September at Lappeenranta (FMI, 2016).

Date/Time	**Cloud coverage (%)**	**Humidity (%)**	**Rain (mm)**
01.09.2016			
00:00	16	88	0.0
03:00	24	90	0.0
06:00	58	92	0.0
09:00	92	89	0.0
12:00	100	87	0.0
15:00	75	82	0.2
18:00	33	76	0.3
21:00	44	83	0.2

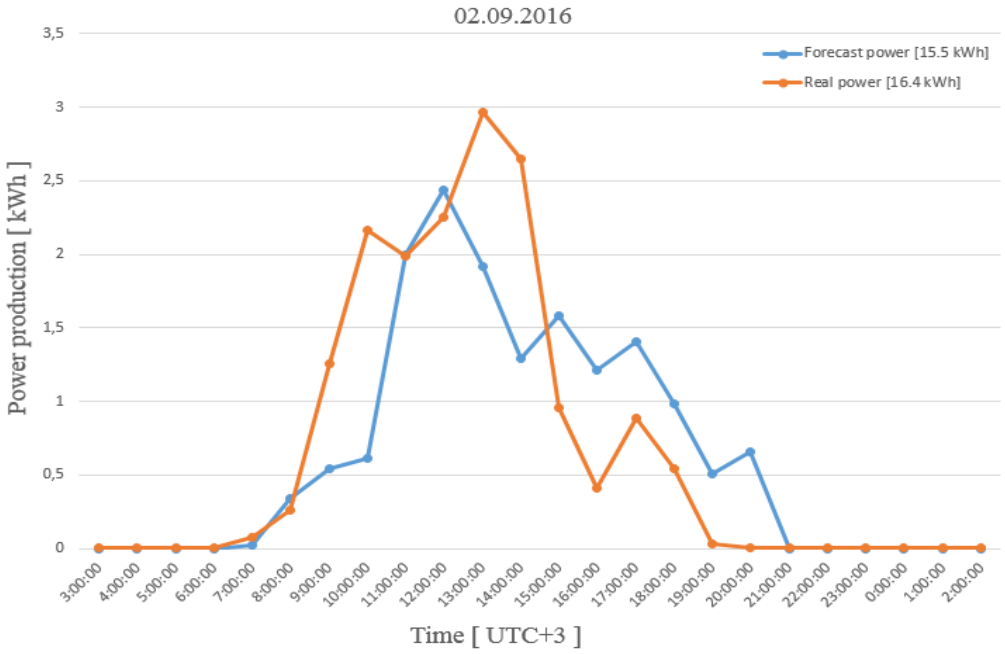

Figure 32: Forecast and real power production on fixed PV system in 02nd September.

As observed from Figure 32, the peak of real power is different from that forecast power with the former being higher. This can be explained by the partial cloud distribution which appears to have minimal impact on the real power produced.

The evaluation of a forecast model is critical in determining its performance. There are several evaluation criteria utilized in determining the performance of forecast models. The most commonly used is the Root Mean Square (RMSE), Mean Absolute Error (MAE) among others. (Şen, 2008). In this study, the Normalized Root Mean Square Error (NRMSE) was employed because of its capability to provide comparative analysis for Photovoltaic Systems (Wu et al., 2014). It is presented as follows in Eq. (22):

$$\mathrm{NRMSE} = \sqrt{\frac{1}{N}\sum_{i=1}^{N}\left(\frac{(P_{\mathrm{HARM.Forecast,i}} - P_{\mathrm{LUT.Realpower,i}}}{P_{\mathrm{install}}}\right)}\ \%\,, \tag{22}$$

where $P_{\mathrm{LUT.Realpower}}$ is a real power production, $P_{\mathrm{HARM.Forecast}}$ the forecast power, P_{install} the PV capacity power installed and N the total number of observation in time horizon.

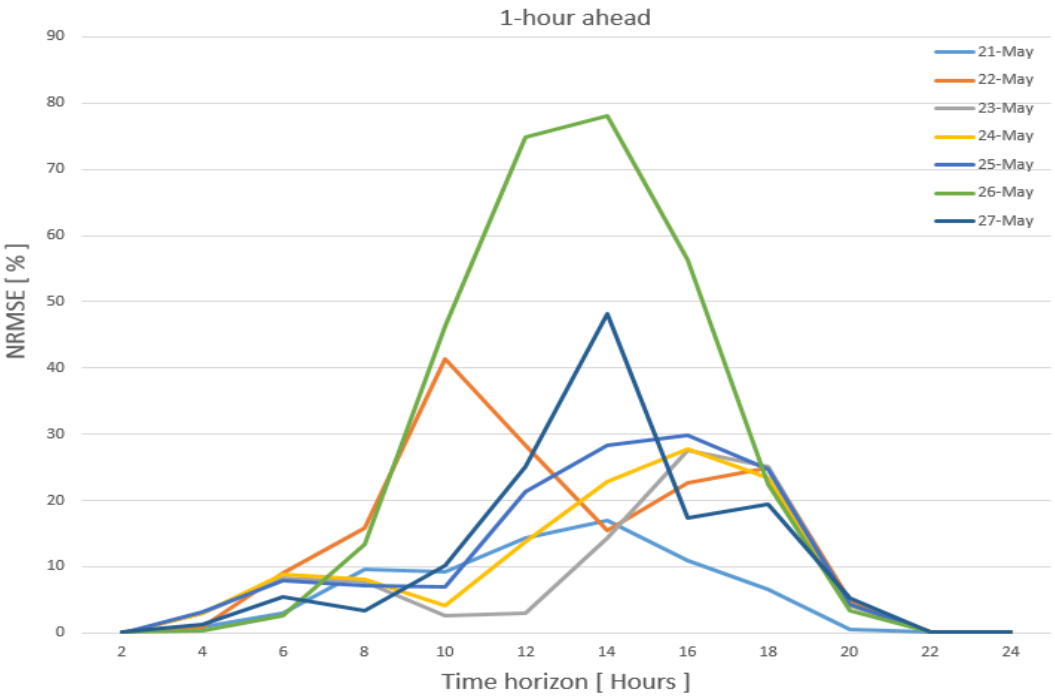

Figure 33: The forecasting accuracy evaluation by a lead time (1-hour ahead).

Figure 33 presents the result errors in terms of NRMSE after evaluation of the forecasting model in a time horizon of one-hour ahead. The NRMSE metric is with respect to real power production measured from the PV power plant at LUT. Chosing the clear days on 23rd and 24th May, the leading errors in the range 0.05% – 27.62% and 0.06% – 27.85% respectively.

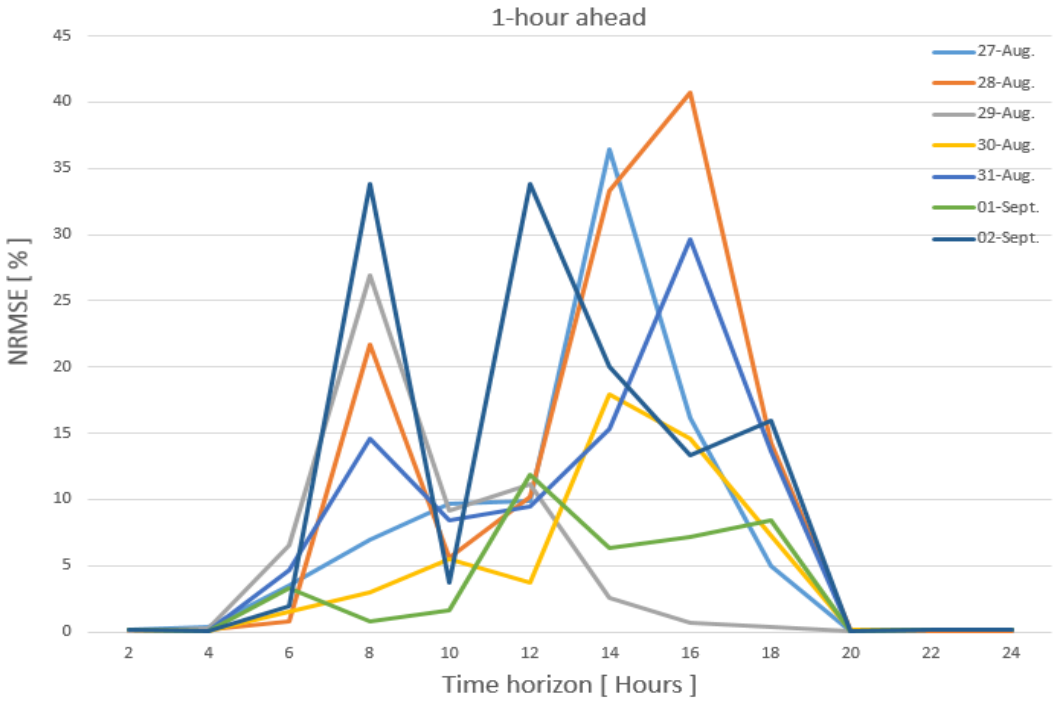

Figure 34: The evaluation of the forecasting accuracy by a lead time (1-hour ahead).

Figure 34 shows the average result errors for the forecasting model after evaluation in a time horizon of one-hour ahead, in terms of NRMSE metric with respect to real power production measured from the PV power plant at LUT. By chosing 29th and 30th August during the rainy and cloud days, the recorded errors are leading in the range of 0.09% – 26.94% and 0.09% – 17.88% respectively.

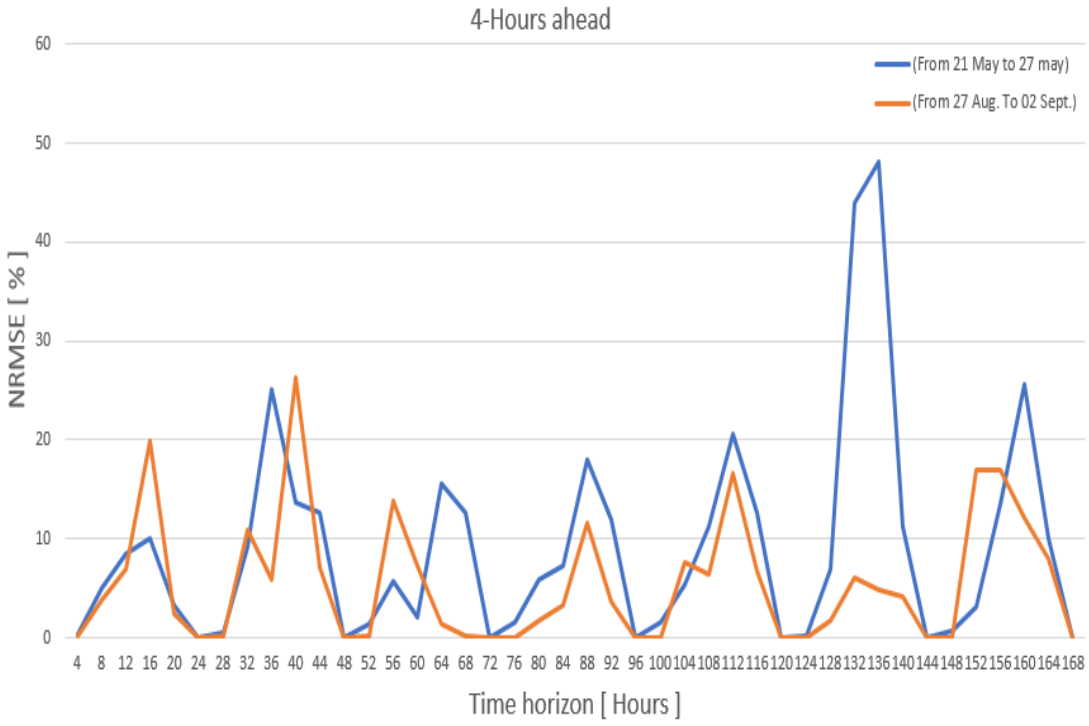

Figure 35: The evaluation of the forecasting accuracy by a lead time (4-hour ahead).

Figure 35 indicates the average result errors after the evaluation of the forecasting model in a time horizon of four-hour ahead, in terms of NRMSE metric with respect to real power production measured from PV system at LUT. The leading errors obtained after chosing 23rd and 24th May during the clear days are leading in the range of 0.06% – 15.55% and 1.54% – 17.10% respectively whereas the errors of 29th and 30th August chosen during the rainy and cloudy days are in the range of 0.08% – 13.86% and 0.07% – 11.54% respectively.

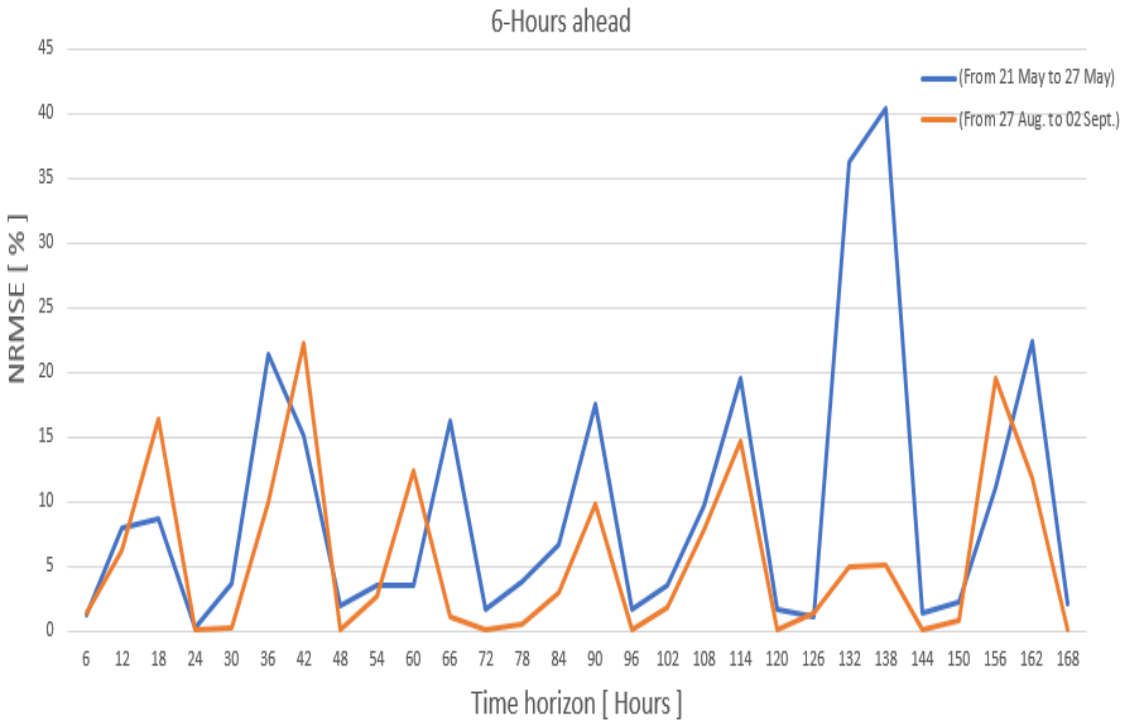

Figure 36: The evaluation of the forecasting accuracy by a lead time (6-hour ahead).

In Figure 36, the average result errors after the evaluation of the forecasting model are shown. The evaluation is done considering the forecast power and the real power in a time horizon of six-hour ahead, in terms of NRMSE metric with respect to real power production measured from PV system at LUT power plant. Both the days of 23rd and 24th May are chosen of which the two days are clear consequently recording a leading error in the range of 3.56% – 16.30% and 3.81% – 17.54% respectively. Similarly on the 29th and 30th August, both of which days are considered during rainy and cloudy days, the leading errors in the range of 0.19% – 12.47% and 0.20% – 9.88% respectively.

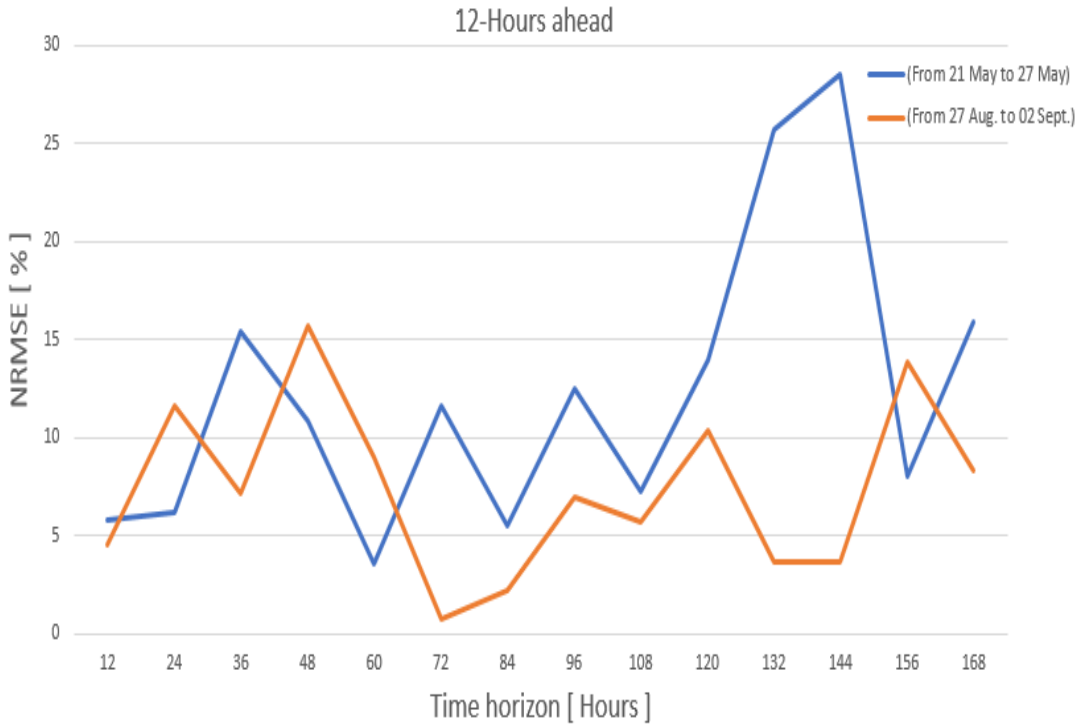

Figure 37: The evaluation of the forecasting accuracy by a lead time (12-hour ahead).

Figure 37, depicts the average result errors of forecasting after the model evaluation in a time horizon of twelve-hour ahead, in terms of NRMSE metric with respect to forecast and real power production measured from PV system at LUT. In this evaluation two intermittent days of 23rd and 24th May were chosen with the leading errors recorded in the range of 3.56% – 11.59% and 5.48% – 12.46% respectively. While in the evaluation of the errors in 29th and 30th August, the leading errors were recorded in the range of 0.77% – 9.02% and 2.15% – 6.98% respectively.

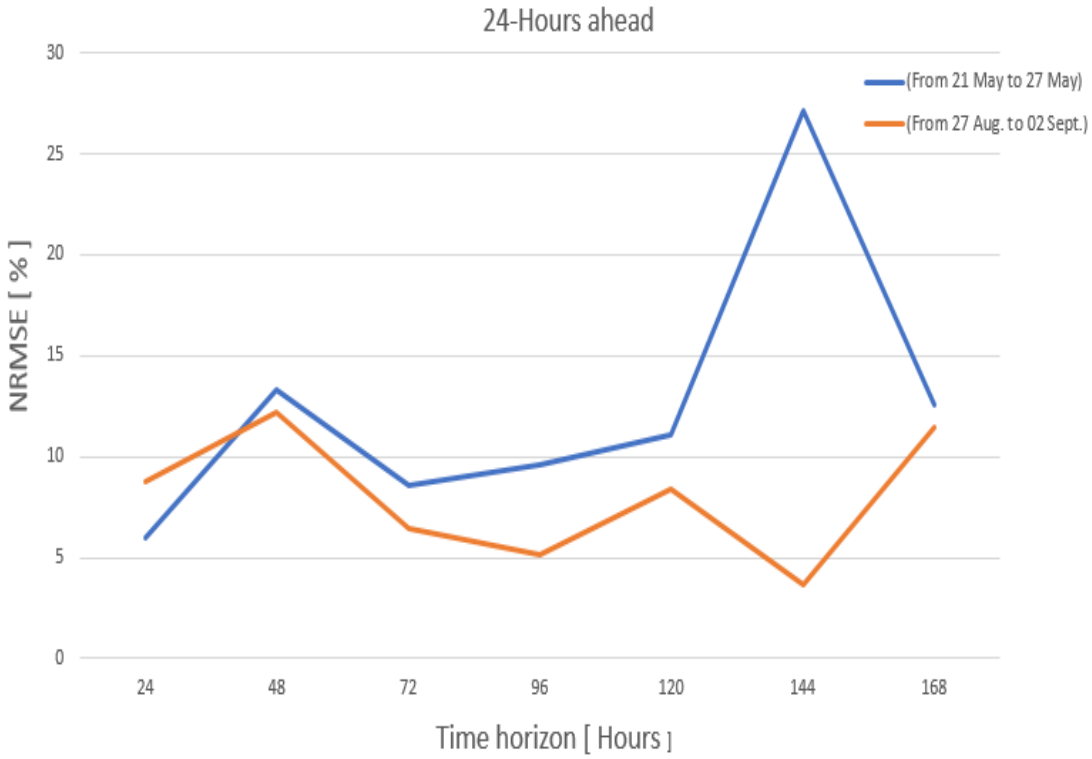

Figure 38: The evaluation of the forecasting accuracy by a lead time (24-hour ahead).

Figure 38 captures the average result errors after the evaluation of the forecasting model in a time horizon of twentyfour-hour ahead, in terms of NRMSE metric with respect to real power production measured from PV system at LUT. Two clear days of 23rd May and 24th May were chosen reporting a respective leading error of 8.57% and 9.63%. A consequent evaluation ensued for the days of the 29th August and 30th August, an evaluation conducted during rainy and cloudy days yielding a respective error of 6.40% and 5.17%. respectively.

5. Discussion

This section provides a description of the results obtained from Section 4. As earlier indicated, the objective of this study was to forecast the PV power output from weather parameters precisely relative humidity, air temperature, wind speed and solar irradiation. The weather variables were obtained from the Lappeenranta University of Technology region weather station as captured in the HARMONIE model which is a subsidiary of the Finnish Meteorological Institute (FMI). The weather data was obtained for two phases, the first containing daily hourly time series data from 21st May 2016 to 27th May 2016 and the second phase consisting of hourly data beginning from 27th August 2016 to 2nd September 2016. The rationale for choosing the data in two phases was two-pronged. During the first phase, the solar irradiation was believed to be at peak, whereas the second phase was considered a rainy season. Thus, analyzing the data in both phases was believed to be of paramount importance towards attaining accurate results for this study. Subsequently, a comparison of the forecasted power output was done with the real power produced from the LUT solar power plant.

In this study, the consideration of the weather parameters which formed the initial phase of the computation of power output was pivotal. Their analysis is believed to have an impact on the solar output. Temperature, total solar irradiation and wind speed obtained from the Harmonie Model were used in the computation of the estimated power output using Eq. (24) in Section 3.3. The total solar irradiation was computed from the beam horizontal irradiation, diffuse horizontal irradiation and global horizontal irradiation using Eq. (12) as shown in subsection 3.2.5.

The obtained estimate power output was then compared with the actual solar output obtained from LUT solar power plant. The visualization of the comparison is depicted using Figure 19 through Figure 38. As observed from the figures, the relationship between the power outputs as computed from our estimation model and the actual power from the solar plant appeared to vary sometimes and be at par at times. A number of factors contributed to these trends in the relationship: weather parameters, time of the day, day of the week, season of the year, among others. As corroborated by Panjwani et al. (2014), some weather variables such as relative humidity, especially in its elevated level, could impact the output of solar power.

As the relationship between the forecast and actual power captured on a fixed PV system is shown in Figure 19, the actual peak power is higher than the forecast peak power. This is as a result of cloud distribution as indicated in Table 1, which appears to occupy the better of the day, thus affecting the intensity of the solar irradiation. A similar illustration can be observed from Figure 31 and 32 with both cases having a deviation between the actual power output and the forecasted power. In both cases, cloud cover appears to affect solar irradiation reaching the surface on of the panels.

Not only does the cloud cover affects the forecasted power, but also does it affect the production of real power. The curve in Figure 19 illustrates this phenomenon, with the cloud cover causing the volatility in the real power produced. In addition to the cloud cover, the efficiency of the inverter which could be influenced by the loss of energy because of its operations could impact the final power output as illustrated in Figure 19.

Less cloudy cover and little rainfall was found to affect the output for both the real power and forecasted power minimally with the maximum peak values realized during such days. Figure 20, which captures the comparison between the real power and forecasted power illustrates such a scenario with maximum peak being realized between 10:00 and 18:00. In similar instances, the forecasted power was higher than the real power as depicted in Figure 24. This is as result of cloud cover and the little rain in addition to the increased cloud intensity during this day as indicated in Table 3, which creates shading on the surface of the panel thus reducing the production of the real power from the PV system.

Despite the minor variations between the forecast power and the actual power, the estimation model was able to forecast power output relatively similar to the real power produced by the solar power plant in LUT. Figure 21 illustrates this scenario, portraying a linear relationship between the forecast power and the real power, which is clearly captured especially in the morning hours. As shown in the Figure, the forecasted power varied linearly with the real power for the better part of the day from 5:00 – 13: 00 with little cloud cover being observed at a range of 4% to 9%.

A similar analogy can be observed in Figure 22 and 26 with the curves representing the forecast and the real power being smooth and steady. As shown in Figure 22 representing 24th May, there was a smooth and stable relationship between the forecasted and real power.

An analogous situation was observed on the 25th May as presented in Figure 23. This was due to the clear sky and the little cloud cover experienced during this day.

Similarly, both Figure 27 and 30 representing the relationship between the forecast power and the real power on 28th August and 31st August respectively, indicates a direct proportion between the forecast power out and the real power output. It is worth noting that in these cases, the relative humidity was significantly low, characterized by cloudless day or little cloud distribution if at all.

Out of the investigated weather parameters consisting of PV panel operating temperature as a function of air temperature, wind speed and solar irradiation. The wind speed was of interest as it played a major role in the estimation of PV power output. As it was observed, the panel temperature decreased with the increase in wind speed.

Rather than just limiting the solar power output, some meteorological parameters could pose other challenges. For instance, according to Elminir et al. (2001), relative humidity and air temperature could cause corrosion to the solar panels, particularly when they are in the range of 60% and 40℃ respectively. Similarly, during humid conditions, especially with the relative humidity being between 75% and 95% with the air temperature being between 20℃ and 40℃, the growth of the fungus could cause the deterioration of the panel cells thus affecting their performance (Elminir et al., 2001).

Furthermore, the formation of the sticky surface of moisture on the panel arising from the humid conditions could lead to accumulation of dirt particles and dust on the panel's surface thus impacting the conversion efficiency of the panels (Elminir et al., 2001). The dirt on the surfaces of the panel could have impacted the findings in this study, however the impact was believed to be minimal to affect the results significantly. Also, the analysis of the extra meteorological parameters was not conducted as it was considered beyond the scope of this thesis. As such, these can be considered areas for further research.

The Figures 33 through 38 as described in Section 4 indicates the average results of evaluating the performance of the forecast model using the NRMSE metric considering the real power production measured from the PV power plant at LUT. As observed from the evaluation, the smaller the errors obtained, the better the forecast model result (Şen, 2008, p. 107–112). Based on our results, the errors decreased as the hours-ahead increased as clearly illustrated in Figure 38 in which evaluation was done on a 24-hour ahead horizon. Moreover,

the clear days of the 23rd May and 24th May provided better results on a 4-hour ahead horizon.

6. Conclusion

The main goal of this research was to forecast solar power energy using a developed model. The study first conceptualized the state of solar irradiation and the potential of solar energy in Finland both of which were presented in the literature review. The research went further to compute power output forecast from weather parameters of temperature, wind speed and total solar irradiation. The total solar irradiation was computed from the beam horizontal irradiation, beam horizontal irradiation and global horizontal irradiation. The obtained power output forecast was then compared with the real power produced from the LUT solar power plant. The efficiency of the model was evaluated using the Normalized Root Mean Square Error (NRMSE) as the evaluation criteria.

The findings indicate that solar power can be forecasted using the weather parameters incorporated in the model. This can be affirmed by the comparison between the forecasted power and the real power produced from LUT solar power plant which was conducted in this study. Despite the few instances of great deviation between the forecasted power and the actual power produced from the solar plant, in many cases there was insignificant or no deviation. In addition, the small errors as indicated by NRMSE especially with hour-ahead time horizon increasing, indicates better performance of the model predicting solar power.

It was also found out that some weather conditions had significant effect on solar power production. In particular, cloudy and rainy periods were found to affect the behavior of solar power production by influencing the intensity of solar irradiation.

In this study, two forms of dataset were used, capturing both the sunny and rainy periods. In the former's case, hourly data from 21st May 2016 to 27th May 2016 was chosen, while in the latter hourly data from 27th August 2016 to 2nd September 2016 was used. Using more data sets capturing the four seasons of winter, spring, summer, and autumn and covering longer periods could have provided broader perspective regarding solar power forecasting. This can indeed be an area of further study.

However, the data set used in this study, constrained to the few weather parameters of temperature, wind speed and solar irradiation has exhibited the possibility of forecasting the solar power using weather parameters as used in the model

References

Bacher, P., Madsen, H. and Nielsen, H.A., 2009. Online short-term solar power forecasting. *Solar Energy, 83*(10), pp.1772–1783.

Benford, F. and Bock, J.E., 1938. *A time analysis of sunshine*. General electric Company, Research laboratory.

Brownson, J. 2016. Empirical correlation for estimating components of Light. Available at: https://www.e-education.psu.edu/eme810/node/683.

Child, M., and Breyer, C., 2016. Vision and initial feasibility analysis of a recarbonised Finnish energy system for 2050. *Renewable and Sustainable Energy Reviews, 66*, pp. 517–536.

Child, M., Haukkala, T. and Breyer, C., 2017. The role of solar photovoltaics and energy storage solutions in a 100% renewable energy system for Finland in 2050. *Sustainability, 9*(8), p. 1358.

Duffie, J.A, and Beckman, W.A., 2013. *Solar engineering of thermal processes*. John Wiley & Sons.

EEA. 2008. Energy and Environment Report 2008. European Environmental Agency report EEA Report No 6/2008, Chap. 2. Available at http://www.eea.europa.eu/.

Elminir, H.K., Benda, V. and Toušek, J., 2001. Effects of solar irradiation conditions and other factors on the outdoor performance of photovoltaic modules. *Journal of electrical engineering-Bratislava*, *52*(5/6), pp.125–133.

EPIA., 2014. European Photovoltaic Industry Association, 2014. Global market outlook for photovoltaics 2014–2018. *Brussels, Belgium*, 60.

Gilbert, M., 2004. Masters, Renewable and efficient electric power systems. *John Wiley & Sons, Inc, New Jersey*, 75, p.76.

Haukkala, T., 2015. Does the sun shine in the High North? Vested interests as a barrier to solar energy deployment in Finland. *Energy Research & Social Science, 6*, pp. 50–58.

HAY, J.E. and McKAY, D.C., 1985. Estimating solar irradiance on inclined surfaces: a review and assessment of methodologies. *International journal of Solar Energy, 3*(4–5), pp. 203–240.

HARMONIE-AROME, R.M., Joint WMO technical progress report on the global data processing and forecasting system and numerical weather prediction research activities for 2011.

Huld, T. and Pascua, I., 2014. Solar radiation and photovoltaic electricity potential country and regional maps for Europe. *European Union, Joint Research Centre*. Available at: http://re.jrc.ec.europa.eu/pvgis/cmaps/eur.htm, [Accessed on May 2014].

IEA. 2009. *World energy outlook,* OECD publication service, OECD, Paris. Available at http://dx.doi.org/10.1787/weo-2009-en.

IEA. (2014). How solar energy could be the largest source of electricity by mid-century, Paris.

Initiatives, P.E., 2014. Who's winning the clean energy race? 2013.

Kleissl, J., 2013. *Solar energy forecasting and resource assessment*. Academic Press.

Klucher, T.M., 1979. Evaluation of models to predict insolation on tilted surfaces. *Solar Energy, 23*(2), pp.111–114.

Koehl, M., Heck, M., Wiesmeier, S. and Wirth, J., 2011. Modeling of the nominal operating cell temperature based on outdoor weathering. *Solar Energy Materials and Solar Cells, 95*(7), pp.1638–1646.

Kosonen, A., Ahola, J., Breyer, C. and Albó, A., 2014, August. Large scale solar power plant in Nordic conditions. In *Power Electronics and Applications (EPE´14-ECCE Europe), 2014 16th European Conference on* (pp.1–10). IEEE.

Kurtz, S., 2012. *Opportunities and challenges for development of a mature concentrating photovoltaic power industry (revision)* (No. NREL/TP-5200–43208). National Renewable Energy Laboratory (NREL), Golden, CO.

Kurtz, S., Whitfield, K., Miller, D., Joyce, J., Wohlgemuth, J., Kempe, M., Dhere, N., Bosco, N. and Zgonena, T., 2009. Evaluation of high-temperature exposure of rack-mounted photovoltaic modules. *In Photovoltaics Specialists Conference (PVSC), 2009 34th IEEE* (pp. 002399–002404). IEEE.

Larson, D.P., Nonnenmacher, L. and Coimbra, C.F., 2016. Day-ahead forecasting of solar power output from photovoltaic plants in the American Southwest. *Renewable energy, 91*, pp. 11–20.

Lorenz, E., Hurka, J., Heinemann, D. Beyer, H.G., 2009. Irradiance forecasting for the power prediction of grid-connected photovoltaic systems. *IEEE Journal of selected topics in applied earth observations and remote sensing, 2*(1), pp. 2–10.

Lorenz, E., Remund, J., Müller, S.C., Traunmüller, W., Steinmaurer, G., Pozo, D., Ruiz Arias, J.A., Lara Fanego, V., Ramirez, L., Gastón, M. and Kurz, C., 2009. Benchmarking of different approaches to forecast solar irradiance.

Lorenz, E., Scheidsteger, T., Hurka, J., Heinemann, D. and Kurz, C., 2011. Regional PV power prediction for improved grid integration. *Progress in Photovoltaics: Research and Applications, 19*(7), pp. 757–771.

Markvart, T. ed., 2000. *Solar electricity* (Vol. 6). John Wiley & Sons.

Mattei, M., Notton, G., Cristofari, C., Muselli, M. and Poggi, P. 2006. Calculation of the polycrystalline PV module temperature using a simple method of energy balance. *Renewable Energy, 31*(4), pp. 553–567.

Myers, D., 2011. *Review of consensus standard spectra for flat plate and concentrating photovoltaic performance* (No. NREL/TP-5500–51865). National Renewable Energy Laboratory (NREL), Golden, CO.

Pandiarajan, N. and Muthu, R., 2011, January. Mathematical modeling of photovoltaic module with Simulink. In *Electrical Energy Systems (ICEES), 2011 1st International Conference on* (pp. 258–263). IEEE.

Panjwani, M.K. and Narejo, G.B., 2014. Effect of humidity on the efficiency of solar cell (photovoltaic). *International journal of engineering research and general science, 2*(4), pp. 499–503.

Pelland, S., Galanis, G. and Kallos, G., 2013. Solar and photovoltaic forecasting through post-processing of the global environmental multiscale numerical weather prediction model. *Progress in photovoltaics: research and applications*, *21*(3), pp. 284–296.

Rekioua, D. and Matagne, E., 2012. *Optimization of photovoltaic power systems: modelization, simulation and control*. Springer Science & Business Media.

Scharmer, K., Greif, J. and Dogniaux, R., 2000. The European solar radiation atlas (Vol. 2, pp.1–296). Les Presses de I´école des mines.

Schwingshackl, C., Petitta, M., Wagner, J.E., Belluardo, G., Moser, D., Castelli, M., Zebisch, M. and Tetzlaff, A., 2013. Wind effect on PV module temperature: Analysis of different techniques for an accurate estimation. *Energy procedia*, *40*, pp.77–86.

Şen, Z., 2008. *Solar energy fundamentals and modeling techniques: atmosphere, environment, climate change and renewable energy*. Springer Science & Business Media.

Skoplaki, E., Boudouvis, A.G. and Palyvos, J.A, 2008. A simple correlation for the operating temperature of photovoltaic modules of arbitrary mounting. *Solar energy materials and solar cells*, *92*(11), pp.1393–1402.

Solmetric Corporation., 2011. Guide to interpreting I-V curve measurements of PV arrays.

Sovacool, B.K., 2009. Rejecting renewables: The socio-technical impediments to renewable electricity in the United States. *Energy policy*, *37*(11), pp. 4500–4513.

Union, E., 2009. Directive 2009/28/EC of the European Parliament and of the Council of 23 April 2009 on the promotion of the use of energy from renewable sources and amending and subsequently repealing Directives 2001/77/EC and 2003/30/EC. *Official Journal of the European Union*, 5, p. 2009.

Värttö, F.A.A.K.M. and Ahoniemi, M., 2009. Finnish energy industries-energy scenarios and visions for the future.

WIRE., 2010. COST Action ES1002 Weather intelligence for renewable energies.

Wu, Y.K., Chen, C.R. and Abdul Rahman, H., 2014. A novel hybrid model for short-term forecasting in PV power generation. *International journal of photoenergy, 2014*.

Yang, D., Jirutitijaroen, P. and Walsh, W.M., 2012. Hourly solar irradiance time series forecasting using cloud cover index. *Solar energy, 86*(12), pp. 3531–3543.

Yona, A., Senjyu, T., Saber, A.Y., Funabashi, T., Sekine, H. and Kim, C.H., 2007. Application of Neural Network to One-Day-Ahead 24 hours generating power forecasting for photovoltaic system. *In intelligent systems applications to power systems, 2007. ISAP 2007. International conference on* (pp.1–6). IEEE.

Appendix 1: Data for specification of PV panel

TWxxxP60-FA

TIANWEI

Polycrystalline Silicon PV Module

Typical Electrical Characteristics at Standard Test Conditions (STC)

Type	Unit	TW230 P60-FA	TW235 P60-FA	TW240 P60-FA	TW245 P60-FA	TW250 P60-FA	TW255 P60-FA
Mpp	P_m (W)	230	235	240	245	250	255
Power Tolerance	W	0 ~ +5	0 ~ +5	0 ~ +5	0 ~ +5	0 ~ +5	0 ~ +5
Max-Power Voltage	V_m (V)	29.4	29.8	30.0	30.4	30.7	31.0
Max-Power Current	I_m (A)	7.82	7.89	8.00	8.06	8.15	8.24
Open-Circuit Voltage	V_{oc} (V)	37.3	37.6	37.6	37.8	38.0	38.2
Short-Circuit Current	I_{sc} (A)	8.22	8.29	8.38	8.50	8.59	8.70
Module Efficiency	η_m (%)	14.14	14.45	14.76	15.06	15.37	15.67
Test Condition	STC:AM=1.5, 1000 W/m², Cells Temperature 25℃						
Operating temperature range	-40℃ ~+85℃						

Mechanical Characteristics

Dimension (L×W×H)	1640 mm x 992 mm x 40 mm
Installation Hole Dimension	860 mm × 942 mm
Weight	19.5 kg
Front cover (material/type/thickness)	Low iron tempered glass 3.2 mm
Cell (quantity/material type/dimensions)	60 (10x6) / Multicrystalline / 156×156 (mm)
Encapsulant (material)	EVA
Frame (material/color)	Anodized aluminum alloy/sliver
Junction box (protection degree)	IP65/IP67
Cable (length/cross-section area)	900 mm/4 mm²

OPERATING CONDITIONS

Max. hailstone impact (diameter/velocity)	25mm hail, form 1m of distance at 23 m/s
Max. system voltage	Dc1000 V (TUV)
Max. series fuse rating	15 A
Operating temperature range	-40 ℃~+85 ℃
Max. static load, front (snow & wind)	5400 Pa
Max. static load, back (wind)	2400 Pa

THERMAL CHARACTERISTICS

Nominal operating temperature	47±2℃
Temperature coefficient of Pmax	- 0.44% / ℃
Temperature coefficient of Voc	- 0.34% / ℃
Temperature coefficient of Isc	0.06% / ℃

Packaging

Container	20Ft (pcs)	40Ft (pcs)	40Hft (pcs)
Modules/pallet	23	23	26
Loading Capacity	276	644	728

Dimensions

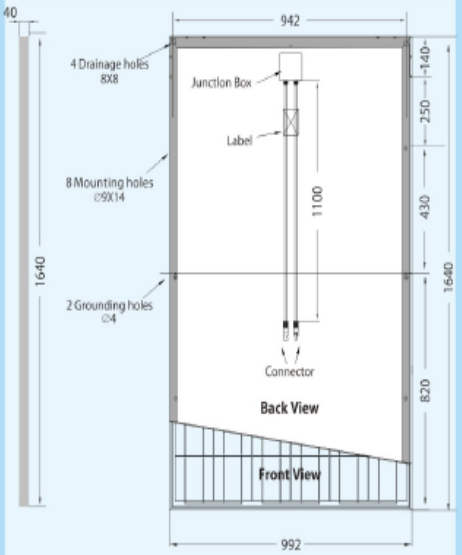

TW235 P60- FA Module IV Curves

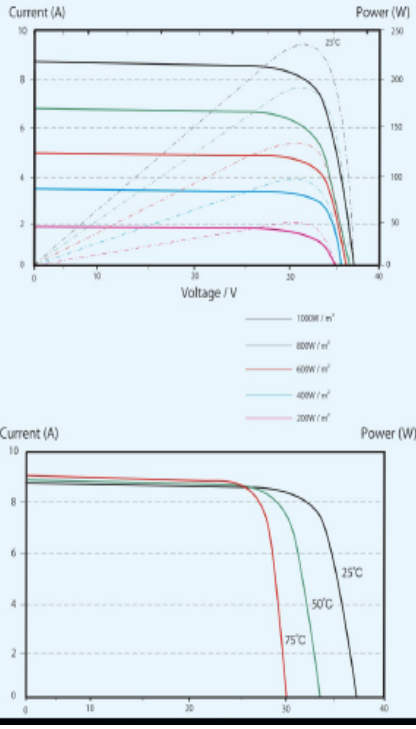

Appendix 2: Data for efficiency of PV-cells materials.

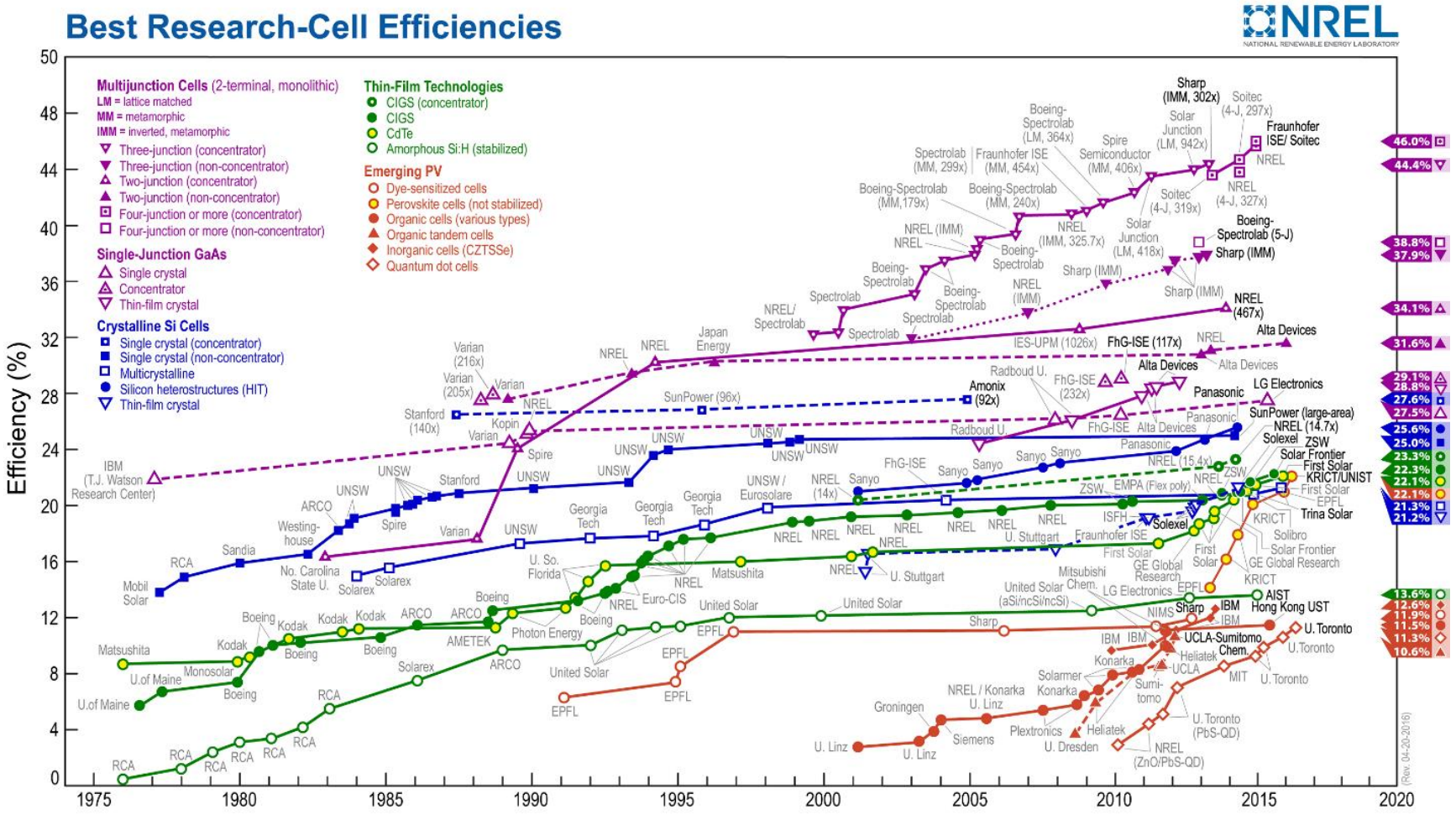

Appendix 3: Excel tool for calculation used PV models.

FIXED MODULES

Date	Time [Hours	Temp[C]	W_speed[m/s	GHI	DHI	Extr_irr.	DNI	Diff_Horz.	Refl_Horz	Solar_Azith	Decl_angle	Hrs_Angle	Incidt_Angle	Incidt degree	Altitude	Tilt_ angl	q/2	Zenith_Degr	Latitude	R_b	A_i	f_k	Grnd albed	A1	A2	A3	Tot_Irr_Tilt
	0:00:00	13	3,31	0	0	0	0	0	0	27,2388744	20,14	-150,97	-0,32161076	108,7603649	-5,49833587	15	8	95,49833587	61,066	3,35651599	#DIV/0!	#DIV/0!	#DIV/0!	#DIV/0!	#DIV/0!	#DIV/0!	#DIV/0!
	1:00:00	12,47	3,03	0,09	0	0	0	0,09	0,09	40,748829	20,14	-135,97	-0,22038917	102,7318921	-1,44605895	15	8	91,44605895	61,066	8,73319182	#DIV/0!	0	1	#DIV/0!	#DIV/0!	0,001533338	#DIV/0!
	2:00:00	11,88	2,84	0,57	0,02	0,52	0,16	0,55	0,05	53,7896703	20,14	-120,97	-0,08725071	95,00546187	3,876186052	15	8	86,12381395	61,066	-1,2906792	0,03846154	0,18731716	0,0877193	-0,05311641	0,5200527	0,000851854	0,46778814
	3:00:00	11,77	2,97	12,39	0	10,96	0	12,39	1,43	66,4905108	20,14	-105,97	0,068731475	86,05886939	10,15814831	15	8	79,84185169	61,066	0,3897098	0	0	0,11541566	0	12,1789105	0,024363034	12,2032735
	4:00:00	11,78	2,82	24,78	0,01	21,94	0	24,77	2,84	79,1164041	20,14	-90,97	0,236927445	76,29473368	17,0764556	15	8	72,9235444	61,066	0,80684294	0,00045579	0,02008859	0,11460856	0,017177591	24,337981	0,048385327	24,4035439
	5:00:00	11,74	3,04	24,04	0	21,3	0	24,04	2,74	92,0507714	20,14	-75,97	0,405874923	66,05403404	24,29616234	15	8	65,70383766	61,066	0,98644223	0	0	0,11397671	0	23,6304284	0,046681618	23,67711
	6:00:00	11,81	3,3	42,46	0	37,67	0,11	42,46	4,79	105,790612	20,14	-60,97	0,56406042	55,6629294	31,45003634	15	8	58,54996366	61,066	1,08108326	0	0	0,11281206	0	41,7366053	0,081607646	41,8182129
	7:00:00	11,81	3,35	67,54	0,06	59,85	0	67,48	7,69	120,932338	20,14	-45,97	0,700703854	45,51649836	38,09995451	15	8	51,90004549	61,066	1,13559777	0,00100251	0,02980541	0,11385845	0,144958059	66,2682328	0,131015198	66,5442061
	8:00:00	11,54	3,49	51,7	0	45,93	0,09	51,7	5,77	138,073224	20,14	-30,97	0,806493202	36,24529077	43,69357588	15	8	46,30642412	61,066	1,16747486	0	0	0,11160542	0	50,8191826	0,098303991	50,9174866
21.5.2016	9:00:00	11,3	3,42	12,12	0	10,98	0,12	12,12	1,14	157,492045	20,14	-15,97	0,874219094	29,04730999	47,56353892	15	8	42,43646108	61,066	1,18453685	0	0	0,09405941	0	11,9135105	0,019422279	11,9329328
	10:00:00	11,26	3,38	20,15	0	18,34	0	20,15	1,81	178,609903	20,14	-0,97	0,899266123	25,93823055	49,06830722	15	8	40,93169278	61,066	1,19030657	0	0	0,0898263	0	19,8067027	0,030837127	19,8375398
	11:00:00	11,05	3,82	19,55	0,06	17,57	0,17	19,49	1,98	160,152862	20,14	14,03	0,879927375	28,36639604	47,9026141	15	8	42,0973859	61,066	1,18587568	0,00341491	0,05539904	0,10127877	0,15008043	19,0948766	0,033733432	19,2786905
	12:00:00	10,59	4,04	19,86	0	17,82	0	19,86	2,04	140,470286	20,14	29,02	0,817575916	35,15713532	44,30912325	15	8	45,69087675	61,066	1,17042476	0	0	0,10271903	0	19,5216435	0,034755657	19,5563991
	13:00:00	10,19	4,37	15,68	0,01	14,38	0,08	15,67	1,3	123,03646	20,14	44,02	0,71637818	44,24373987	38,90013095	15	8	51,09986905	61,066	1,14079346	0,00069541	0,02525381	0,08290816	0,023839251	15,3931818	0,022148213	15,4391693
	14:00:00	9,98	3,9	18,79	0	16,74	0,03	18,79	2,05	107,66628	20,14	59,02	0,583258178	54,31996668	32,35349361	15	8	57,64650639	61,066	1,08991437	0	0	0,10910059	0	18,4698731	0,034926028	18,5047992
	15:00:00	9,9	3,26	20,06	0,1	18,11	0	19,96	1,95	93,7795422	20,14	74,02	0,427287818	64,70443902	25,23832027	15	8	64,76167973	61,066	1,00211889	0,00552181	0,07060485	0,09720837	0,210660773	19,5146657	0,033222319	19,7585488
	16:00:00	9,62	3,17	10,48	0	9,27	0,04	10,48	1,21	80,7709696	20,14	89,02	0,259096223	74,98355804	18,00534149	15	8	71,99465851	61,066	0,83821249	0	0	0,11545802	0	10,3014513	0,020614875	10,3220662
	17:00:00	9,38	2,98	9,58	0,1	8,81	0	9,48	0,77	68,1290847	20,14	104,02	0,090145371	84,82802975	11,02851637	15	8	78,97148363	61,066	0,47123123	0,01135074	0,10216855	0,08037578	0,097829957	9,21480984	0,013118557	9,32575835
	18:00:00	9,19	2,76	9,74	0	8,45	0,13	9,74	1,29	55,4556128	20,14	119,02	-0,06805101	93,9020516	4,64538198	15	8	85,35461802	61,066	-0,8402562	0	0	0,13244353	0	9,57405877	0,021977842	9,59603662
	19:00:00	9,02	2,87	4,3	0	3,91	0	4,3	0,39	42,4694121	20,14	134,02	-0,20471211	101,812647	-0,81960493	15	8	90,81960493	61,066	14,3112122	0	0	0,09069767	0	4,22674053	0,006644464	4,23338499
	20:00:00	8,92	1,98	0,02	0	0,06	0,09	0,02	-0,04	29,0223356	20,14	149,02	-0,3105247	108,090854	-5,05354095	15	8	95,05354095	61,066	3,52522002	0	0	-2	0	0,01965926	-0,00068148	0,01897777
	21:00:00	8,67	2,38	0,05	0,04	0	0	0,01	0,05	15,1215764	20,14	164,02	-0,37827781	112,2270471	-7,77772221	15	8	97,77772221	61,066	2,7952181	#DIV/0!	0,89442719	1	#DIV/0!	#DIV/0!	0,000851854	#DIV/0!
	22:00:00	8,4	2,14	0,05	0	0	0,18	0,05	0,05	0,93100764	20,14	179,02	-0,4033542	113,7880337	-8,79014799	15	8	98,79014799	61,066	2,6394778	#DIV/0!	0	1	#DIV/0!	#DIV/0!	0,000851854	#DIV/0!
	23:00:00	11,95	0,35	0	0	0	0,01	0	0	13,2787284	20,14	194,02	-0,38404494	112,5844615	-8,01033421	15	8	98,01033421	61,066	2,7559399	#DIV/0!	#DIV/0!	#DIV/0!	#DIV/0!	#DIV/0!	#DIV/0!	#DIV/0!
	0:00:00	11,58	0,93	0	0	0	0	0	0	27,1823486	20,34	-150,98	-0,31857471	108,5767511	-5,30618701	15	8	95,30618701	61,066	3,44486615	#DIV/0!	#DIV/0!	#DIV/0!	#DIV/0!	#DIV/0!	#DIV/0!	#DIV/0!
	1:00:00	10,91	1,36	0	0	0	0	0	0	40,6727072	20,34	-135,98	-0,21750714	102,5626572	-1,26086515	15	8	91,26086515	61,066	9,88467867	#DIV/0!	#DIV/0!	#DIV/0!	#DIV/0!	#DIV/0!	#DIV/0!	#DIV/0!
	2:00:00	10,12	0,68	13,65	3,72	11,83	62,66	9,93	1,82	53,6977566	20,34	-120,98	-0,08455836	94,85062939	4,05417569	15	8	85,94582431	61,066	-1,1960218	0,31445478	0,52204164	0,13333333	-8,183822	6,69925292	0,031007498	-1,4535616
	3:00:00	9,93	0,74	71,84	17,79	62,85	161,76	54,05	8,99	66,3860466	20,34	-105,98	0,071211381	85,91643209	10,32996336	15	8	79,67003664	61,066	0,39712627	0,28305489	0,497628	0,1251392	13,14055762	38,1328327	0,153163411	51,4265538
	4:00:00	10,37	0,32	99,41	0	87	0,03	99,41	12,41	78,9934991	20,34	-90,99	0,239073111	76,16815891	17,23943147	15	8	72,76056853	61,066	0,80668358	0	0	0,12483654	0	97,7163432	0,211430248	97,9277734
	5:00:00	12,09	0,35	175,29	3,57	153,47	8,95	171,72	21,82	91,9199616	20,34	-75,99	0,407810012	65,93266278	24,45789017	15	8	65,54210983	61,066	0,9849904	0,02326188	0,14271037	0,12447943	7,4509887	164,920239	0,371749235	172,742977
	6:00:00	13,17	1,37	280,45	20,87	245,38	44,5	259,58	35,07	105,655033	20,34	-60,99	0,565813788	55,54117868	31,61434699	15	8	58,38565301	61,066	1,07938705	0,08505176	0,27279318	0,12504903	46,35722886	233,597541	0,597490636	280,55226
22.5.2016	7:00:00	13,63	1,68	389,2	35,54	340,5	61,78	353,66	48,7	120,798307	20,34	-45,99	0,702316744	45,38682652	38,27099124	15	8	51,72900876	61,066	1,13389988	0,10437592	0,30218458	0,12512847	82,15511343	311,559202	0,82970613	394,544022
	8:00:00	14,41	1,83	532,24	133,1	466,19	197,68	399,14	66,05	137,953269	20,34	-30,99	0,808016428	36,09741869	43,87482773	15	8	46,12517227	61,066	1,16582555	0,28550591	0,50007515	0,12409815	288,0251629	280,636218	1,125299587	569,786681
	9:00:00	13,68	1,51	278,08	25,5	243,5	36,29	252,58	34,58	157,406014	20,34	-15,99	0,875709581	28,87093413	47,75587857	15	8	42,24412143	61,066	1,18293237	0,10472279	0,30282046	0,1243527	61,45438091	222,426218	0,589142463	284,469742
	10:00:00	15,84	0,83	526,67	324,94	461,34	428,86	201,73	65,33	178,577334	20,34	-0,99	0,900783028	25,73881564	49,26805372	15	8	40,73194628	61,066	1,18872782	0,70433953	0,78547487	0,12404352	555,1672905	58,7298393	1,113032884	615,010163
	11:00:00	15,79	1,65	506,51	220,76	443,33	292,03	285,75	63,18	160,128113	20,34	14,01	0,881528053	28,17275552	48,10280879	15	8	41,89719121	61,066	1,1843015	0,49795863	0,6601858	0,12473594	429,9626483	141,221234	1,076403148	572,260285
	12:00:00	16,09	1,82	570,51	325,8	499,67	444,94	244,71	70,84	140,390735	20,34	29,01	0,819256852	34,98952913	44,50110795	15	8	45,49889205	61,066	1,16882566	0,65203034	0,75569041	0,1241696	567,2992861	83,8415782	1,206907233	652,347772
	13:00:00	16,42	1,32	433,33	243,51	379,57	353,33	189,82	53,76	122,936046	20,34	44,01	0,718213105	44,09285256	39,08451384	15	8	50,91548616	61,066	1,13917811	0,64154174	0,74963356	0,12406249	416,1274732	66,9947954	0,915913789	484,038182
	14:00:00	17,11	2,22	444,64	318,82	389,25	553,43	125,82	55,39	107,55949	20,34	59,01	0,585282775	54,17703073	32,53228372	15	8	57,46771628	61,066	1,08834189	0,8190623	0,84677595	0,12457269	459,1436021	22,4198607	0,943684241	482,507147
	15:00:00	16,99	2,2	451,99	354,45	395,52	724,67	97,54	56,47	93,6745894	20,34	74,01	0,429524845	64,56259062	25,41463995	15	8	64,58536005	61,066	1,0008363	0,89616201	0,88554998	0,12493639	442,2311697	9,97540509	0,962084295	453,168659
	16:00:00	16,37	2,34	327,2	241,77	285,73	644,41	85,43	41,47	80,6723924	20,34	89,01	0,26155396	74,83771136	18,18228183	15	8	71,81771817	61,066	0,83820347	0,84614846	0,85959634	0,12674205	263,2432162	12,9443059	0,706527992	276,89405
	17:00:00	15,83	2,01	204,97	139,51	178,84	537,46	65,46	26,13	68,0399754	20,34	104,01	0,092817059	84,67430868	11,20863541	15	8	78,79136459	61,066	0,47749774	0,78008276	0,82500678	0,12748207	90,99875846	14,1764817	0,44517908	105,620419
	18:00:00	15,19	1,02	97,29	52,43	84,83	355,74	44,86	12,46	55,3874589	20,34	119	-0,06508741	93,73187216	4,834429285	15	8	85,16557071	61,066	-0,7723068	0,61805965	0,73410102	0,12807072	-61,9051464	16,8694275	0,212282102	-44,823437
	19:00:00	14,47	0,26	21,65	6,87	18,71	103,62	14,78	2,94	42,4174027	20,34	134	-0,201608	101,6310064	-0,62557508	15	8	90,62557508	61,066	18,4654368	0,36718332	0,56331254	0,13579677	227,0689139	9,20519887	0,050089035	236,324202
	20:00:00	12,55	0,5	0	0,07	-0,01	0	-0,07	0,01	28,9903775	20,34	149	-0,30733088	107,8984506	-4,85520179	15	8	94,85520179	61,066	3,63112699	-7	#DIV/0!	#DIV/0!	2,033431117	#DIV/0!	#DIV/0!	#DIV/0!
	21:00:00	13,28	0,8	0,1	0	0	0,1	0,1	0,1	15,1132002	20,34	164	-0,37505122	112,0274787	-7,57701542	15	8	97,57701542	61,066	2,84434086	#DIV/0!	0	1	#DIV/0!	#DIV/0!	0,001703709	#DIV/0!
	22:00:00	12,58	0,52	0	0	0	0,12	0	0	0,94827905	20,34	179	-0,40015398	113,5878052	-8,58999646	15	8	98,58999646	61,066	2,67907556	#DIV/0!	#DIV/0!	#DIV/0!	#DIV/0!	#DIV/0!	#DIV/0!	#DIV/0!
	23:00:00	11,09	1,56	0	0	0	0	0	0	13,2360386	20,34	194	-0,38092846	112,3912055	-7,8139564	15	8	97,8139564	61,066	2,8018325	#DIV/0!	#DIV/0!	#DIV/0!	#DIV/0!	#DIV/0!	#DIV/0!	#DIV/0!